An Improved Coarse-Mesh Nodal Integral Method for Partial Differential Equations

Rizwan-uddin*†
Department of Nuclear Engineering, University of Illinois at Urbana-Champaign, 214 NEL, 103 S. Goodwin Avenue, Urbana, Illinois 61801

Received 4 April 1996; accepted: 14 August 1996

An improved variation of the nodal integral method to solve partial differential equations has been developed and implemented. Rather than treating *all* of the nonlinear terms as the so-called pseudo-source terms (to be approximated), in this modified version of the nodal integral method, by approximating part of the nonlinear terms in terms of the discrete variable(s) that ultimately result at the end of the formulation process, some or all of the nonlinear terms are kept on the left-hand side in the transverse-integrated equations, which are to be solved analytically. Application of the method to solve the Burgers equation leads to exponential variation within the nodes and shows that the resulting scheme has inherent upwinding. Reconstruction of node interior solution —as a function of one independent variable, and averaged in all others —makes it possible to obtain rather accurate solutions even on a fine scale. Results of the numerical analysis and comparison with results of other methods reported in the literature show that the new method is comparable and sometimes better in accuracy than the currently used schemes. Extension to multidimensional problems is straightforward.

Keywords: Coarse-mesh; nonlinear PDEs; Burgers equation; inherent upwinding

I. INTRODUCTION

Nodal integral methods have been developed and used to solve steady-state and time-dependent, multidimensional problems in heat transfer, fluid flow, neutron diffusion, plasma physics, etc. The *nodal integral method* (NIM), when applied to solve the linear, two-dimensional, steady-state convection–diffusion equation [1, 2], leads to inherent upwinding in the final set of the discretized equations; that is, the magnitude of the coefficients of the unknown variables in the set of discretized equations depend upon the flow direction to account for the appropriate *influence* of neighboring nodes on each other. On the other hand, as desirable a characteristic as inherent upwinding was not present in other earlier developments of the NIM for problems such as the Navier–Stokes equation, Burgers equation, etc. In this article, we present a modified nodal integral

* Also Computational Science and Engineering Program.
† Work performed while at the University of Virginia.

Numerical Methods for Partial Differential Equations 13, 113—145 (1997)
 CCC 0749-159X/97/020113-33

method that leads to inherent upwinding in the final set of discretized equations —and, hence, to a more accurate numerical scheme—even for problems for which the conventional nodal integral method shows no inherent upwinding.

After the summary of the article a brief background of the conventional NIM, outlining the spirit behind it and important steps in its formulation, is given in the next section. The new modified formalism is outlined in the context of Burgers equation. Though application of the modified NIM to Navier–Stokes equation is conceptually similar and desirable (though nontrivial for time-dependent Navier–Stokes equations in three space dimensions), Burgers equation has often been used as a convenient *simplified* form of the Navier–Stokes equation to test and present properties of numerical methods for several reasons. Without repeating those here—well explained by Fletcher [3]—we also *adopt* the one-dimensional time-dependent Burgers equation as our test problem. In Section III, we formulate the modified NIM for Burgers equation. A condensed version of the conventional NIM formalism is reproduced in Appendix A from Ref. 4. It is shown in Appendix B that the new formalism, which is actually a generalization of the conventional one, reduces to the conventional formulation in the limit of small cell Reynolds number. Results of the numerical solution of one steady-state and two time-dependent problems are presented, and properties of the new formalism are discussed in Section IV on *Numerical Examples.*

II. BACKGROUND AND MOTIVATION

Coarse-mesh nodal methods, including nodal integral methods (NIMs), have been developed over the last two decades to efficiently solve sets of linear and nonlinear PDEs [5–12, 4]. Among the distinguishing features of some of the coarse mesh methods is the transverse integration process that—after the problem domain has been divided into nodes—reduces each of the PDE to an ODE by integrating over the node dimensions of all-but-one independent variables [6–8, 10]. Carrying out the procedure repeatedly, one obtains a set of m ODEs for each PDE, where m is the number of the independent variables. The set of ODEs can usually be solved more easily than the original PDEs.

The distinguishing feature of the *nodal integral method* (NIM)—which is one of the coarse-mesh methods—is the analytical solution of as *much* of the ODEs (obtained after the transverse integration procedure) as possible [9, 10]. The details of this step will become more clear in the next section. Since closed form exact solutions of the set of ODEs are, in general, not possible, part of this step is only performed formally: the *linear* part of the ODEs is solved while the nonlinear terms are treated as inhomogeneous terms (traditionally called the *pseudo-source* term) with particular solutions written out for them. The fact that part of the ODEs (the linear part) is solved exactly ensures that the fundamental solutions are relevant to the problem, leading to linear, quadratic, trigonometric, or exponential (hyperbolic) solutions *as dictated by a portion of the governing equations.* This should be contrasted with other methods, including Fourier, collocation, spectral etc., in which the solution is essentially expanded in a fixed basis independent of the problem and its needs. For example, a method that, say, expands the spatial solution in trigonometric functions is expected to perform well even with a small number of terms in the expansion when the solution is spatially oscillating, but will need significantly more terms to accurately represent an exponentially varying solution. This approach of solving part of the equation analytically allows the NIM to yield a rather accurate solution even with only a few terms in the *expansion.*

The dependent variables in transverse-averaged ODEs are the original dependent variables, each locally averaged over $(m-1)$ directions. Each ODE is written with the analytically solvable part on the left-hand side (usually the linear terms), and all the other terms are grouped on the

right-hand side in the *pseudo-source term.* The pseudo-source terms are now expanded in, for example, Legendre polynomials, truncated at a certain order, and the explicit solution for the ODEs are written for each node. The number of terms kept in the expansion determines the order of the final numerical scheme. Imposing continuity and/or other physical conditions at node interfaces leads to a template that relates averaged quantities on nearby surfaces. Since the pseudo-source terms were never formally evaluated, the coefficients in their expansion also appear as unknowns in the final set of discretized equations. Hence, more equations are needed to complete the development. Traditionally, these extra equations are obtained by imposing two rather important and physically relevant conditions [9, 10]. First, each PDE is integrated over a node, and an equation that relates the averaged pseudo-sources is obtained. This equation ensures that the final numerical scheme is conservative. The second set of necessary equations is obtained by requiring that node averaged value of each dependent variable should be independent of the order in which integration is carried out. Specifically, if temperature is being calculated by solving the steady-state, convection–diffusion heat equation, then $\bar{T}^{xy}_{i,j} = \bar{T}^{yx}_{i,j}$, where $\bar{T}^{xy}_{i,j}$ is the average temperature in node (i, j) obtained by integrating $T(x, y)$ first in the x direction and then in the y direction, and $\bar{T}^{yx}_{i,j}$ is obtained by integrating first in the y direction and then in the x direction. Unless explicitly imposed, there is no guarantee that results of the numerical scheme will have this property [9, 10]. These additional equations that relate the surface averaged quantities and the source terms close the set of equations. For some problems, the pseudo-sources (or the coefficient of their expansions) appear in the final set in a form that makes it possible to algebraically eliminate some or all of them, thereby reducing the number of equations to be solved per node.

In the conventional NIM solution of the Navier–Stokes equation and that of Burgers equation, the convection term, being nonlinear, is moved over to the right-hand side, becomes a part of the pseudo-source term, and, as a result, gets approximated when the pseudo-source term is expanded in Legendre polynomials. Clearly these nonlinear terms, which are approximated by a constant (for a second-order method) or by a linear term (for a third-order method) in the independent variable, play only a minor role in the most important characteristic of the NIM; namely, in determining the form of the analytical solution of (a part of) the original equation. On the other hand, the convection term in the steady-state convection–diffusion equation–when that is solved for a given flow field–is linear and is, hence, retained on the left-hand side, leading to a much more accurate solution within the node. Specifically, while the conventional application of the NIM to two-dimensional steady-state Navier–Stokes equation leads to parabolic velocity distribution within the node [9, 10], application to the linear convection–diffusion equation leads to exponential solutions [1, 2]. For the two-dimensional steady-state convection–diffusion equation for temperature, these exponential solutions are for the y-dependent x-averaged temperature $\bar{T}^x(y)$, and for the x-dependent y-averaged temperature $\bar{T}^y(x)$. Application of the rest of the steps in the NIM then leads to a discretized set that has inherent upwinding. Hence, if the convection term is retained *in some form* in the analytical solution step of the NIM formalism, the resulting scheme will have the upwinding characteristic.

Introduction of any approximation in the conventional NIM was postponed as far down in the procedure as possible. Though this results in a very elegant development [9, 10], when the approximations are made at a late stage, as expected, they obviously lead to some error in the final solution, but more importantly at this late stage they cannot influence the fundamental nature of the analytical solution within each node. The example of the steady-state convection–diffusion problem with known flow field [1, 2] suggests that even when the flow field is not known, it is probably better to approximate the convection term at least partially so that it can be a part of the equation that is solved exactly (as it was in the convection–diffusion equation), hence leading to the desirable exponential solutions and the upwinding associated with them.

Realizing that the nonlinear convection term will become a part of the pseudo-source term, which will be expanded and truncated any way, we introduce the approximation even before solving the transverse integrated equations. Consider, for example, the Burgers equation averaged over 2τ (from $-\tau$ to $+\tau$):

$$\frac{1}{2\tau}\int_{-\tau}^{+\tau}\left[\left(\frac{1}{Re}\right)\frac{\partial^2 u(x,t)}{\partial x^2} - u(x,t)\frac{\partial u(x,t)}{\partial x} - \frac{\partial u(x,t)}{\partial t}\right] dt = 0.$$

Rather than making the nonlinear term a part of the pseudo-source term, we retain it on the left-hand side and realize that the approximation

$$\frac{1}{2\tau}\int_{-\tau}^{+\tau} u(x,t)\frac{\partial u(x,t)}{\partial x}\, dt \simeq \left[\frac{1}{2\tau}\int_{-\tau}^{+\tau} u(x,t)\, dt\right]\left[\frac{1}{2\tau}\int_{-\tau}^{+\tau}\frac{\partial u(x,t)}{\partial x}\, dt\right]$$

is a second-order approximation [9], which yields

$$\frac{1}{Re}\frac{d^2\bar{u}^t(x)}{dx^2} - \bar{u}^t(x)\frac{\partial \bar{u}^t(x)}{\partial x} = \frac{1}{2\tau}\int_{-\tau}^{\tau}\frac{\partial u(x,t)}{\partial t}\, dt.$$

The last approximation is made even in conventional NIM, though at a later stage. The equation above must be solved for the analytical solution of the NIM within each node. The nonlinear equation in the modified nodal integral method (MNIM) is solved by assuming the time-averaged velocity $\bar{u}^t(x)$ (that multiplies the spatial derivative of the time-averaged velocity in the nonlinear term) to be a constant, equal to the average of the time-averaged velocities at the left and right surfaces of the node (over which the spatial integration is to take place). The nonlinear term, in its approximated form, stays on the left-hand side, contributes toward the selection of the solution within the nodes, and leads to upwinding in the final set of discretized equations, and consequently better numerical scheme.

Note that we do not at this point know the average of the time-averaged velocity at the two spatial surfaces of each node. But that does not limit the application of this method in any way. The constant introduced in each node is a simple function of some of the unknowns that result in the final discretized set of equations, and, hence, can be simultaneously solved for with the rest of the unknowns at the end of the formulation process. It is this *early* approximation of the nonlinear term that distinguishes the modified NIM from the conventional NIM. This approximation in some form is made even in conventional NIM, but, made at this stage, it results in more of the original (now approximate) equation participating in the determination of the form of the analytical solution within each node, which is hence more representative of the actual physics of the nonlinear problem.

III. FORMALISM

Burgers equation has often been used as a *model for all reasons* [3, 13], and several researchers have used it as a benchmark for accurate comparison of numerical schemes [14–17]. To demonstrate the improvement over conventional NIM, and to compare the MNIM with other schemes, we apply the improved NIM to one-dimensional, time-dependent Burgers equation

$$\frac{\partial u(x,t)}{\partial t} + u(x,t)\frac{\partial u(x,t)}{\partial x} - \frac{1}{Re}\frac{\partial^2 u(x,t)}{\partial x^2} = 0. \tag{1}$$

For comparison purposes, the corresponding steps for the conventional NIM as applied to the one-dimensional, time-dependent Burgers equation are presented in Appendix A [4].

The spatial domain $x_\ell \le x \le x_r$ is divided into n_x spatial nodes indexed with subscript i. The solution will be calculated at time intervals of 2τ. Time is indexed with subscript j. The schematic of the nodalization scheme is shown in Fig. 1. Each space–time node is of width $2a_{i,j}$ and height 2τ. A local coordinate system [Fig. 1(b)] is defined within each node (i, j) with origin at the node center. Transverse integrating Burgers equation over the node (i, j) over each one of the independent variables (x and t here), i.e., operating the PDE with $\frac{1}{(2a_{i,j})}\int_{-a_{i,j}}^{+a_{i,j}} dx$ and with $\frac{1}{(2\tau)}\int_{-\tau}^{\tau} dt$, we obtain the space-averaged time-dependent equation,

$$\frac{d\bar{u}^x(t)}{dt} = \bar{S}_1^x(t) \equiv \frac{1}{(2a_{i,j})}\int_{-a_{i,j}}^{+a_{i,j}} \left[\frac{1}{Re}\frac{\partial^2 u(x,t)}{\partial x^2} - u(x,t)\frac{\partial u(x,t)}{\partial x}\right] dx, \tag{2}$$

and the time-averaged space-dependent equation,

$$\frac{1}{Re}\frac{d^2\bar{u}^t(x)}{dx^2} - \bar{u}^t(x)\frac{d\bar{u}^t(x)}{dx} = \bar{S}_2^t(x) \equiv \frac{1}{(2\tau)}\int_{-\tau}^{\tau} \frac{\partial u(x,t)}{\partial t}\, dt, \tag{3}$$

where it is understood that these are local integrations over the node (i, j), and, hence, the subscript (i, j) must appear on transverse integrated quantities (dropped here for convenience), and

$$\bar{u}_{i,j}^x(t) \equiv \frac{1}{(2a_{i,j})}\int_{-a_{i,j}}^{+a_{i,j}} u(x,t)\, dx \tag{4}$$

and

$$\bar{u}_{i,j}^t(x) \equiv \frac{1}{(2\tau)}\int_{-\tau}^{+\tau} u(x,t)\, dt. \tag{5}$$

Over each node, $\bar{u}_{i,j}^t(x)$ represents the time-averaged but space-dependent velocity, and $\bar{u}_{i,j}^x(t)$ represents space-averaged but time-dependent velocity. See Fig. 1(b). Equations (2) and (3) are now solved. Treatment of the space-averaged time-dependent equation, Eq. (2), is similar to that in the conventional NIM. The pseudo-source term is expanded in Legendre polynomials and truncated at zeroth order—leading to a constant—and the first order ODE,

$$\frac{d\,\bar{u}^x(t)}{dt} = \bar{S}_1^{x,t}, \tag{6}$$

is simply integrated from $t = -\tau$ to t,

$$\bar{u}^x(t) = \bar{u}^x(-\tau) + \bar{S}_1^{x,t}(\tau + t). \tag{7}$$

When evaluated at $t = +\tau$, it results in

$$\bar{u}^x(\tau) = \bar{u}^x(-\tau) + 2\tau\bar{S}_1^{x,t},$$

which relates the space-averaged solution for node (i, j) at two successive time steps. Obviously, the constant source term needs to be evaluated using the additional constraints discussed earlier. The last equation, written in terms of subscripts (i, j), becomes

$$\bar{u}_{i,j}^x = \bar{u}_{i,j-1}^x + 2\tau\bar{S}_{1,(i,j)}^{x,t}. \tag{8}$$

This completes the solution of the space-averaged equation.

We now expand the pseudo-source term in Eq. (3), truncate it at zeroth order,

$$\frac{1}{Re}\frac{d^2\bar{u}^t(x)}{dx^2} - \bar{u}^t(x)\frac{d\,\bar{u}^t(x)}{dx} = \bar{S}_2^{t,x}, \tag{9}$$

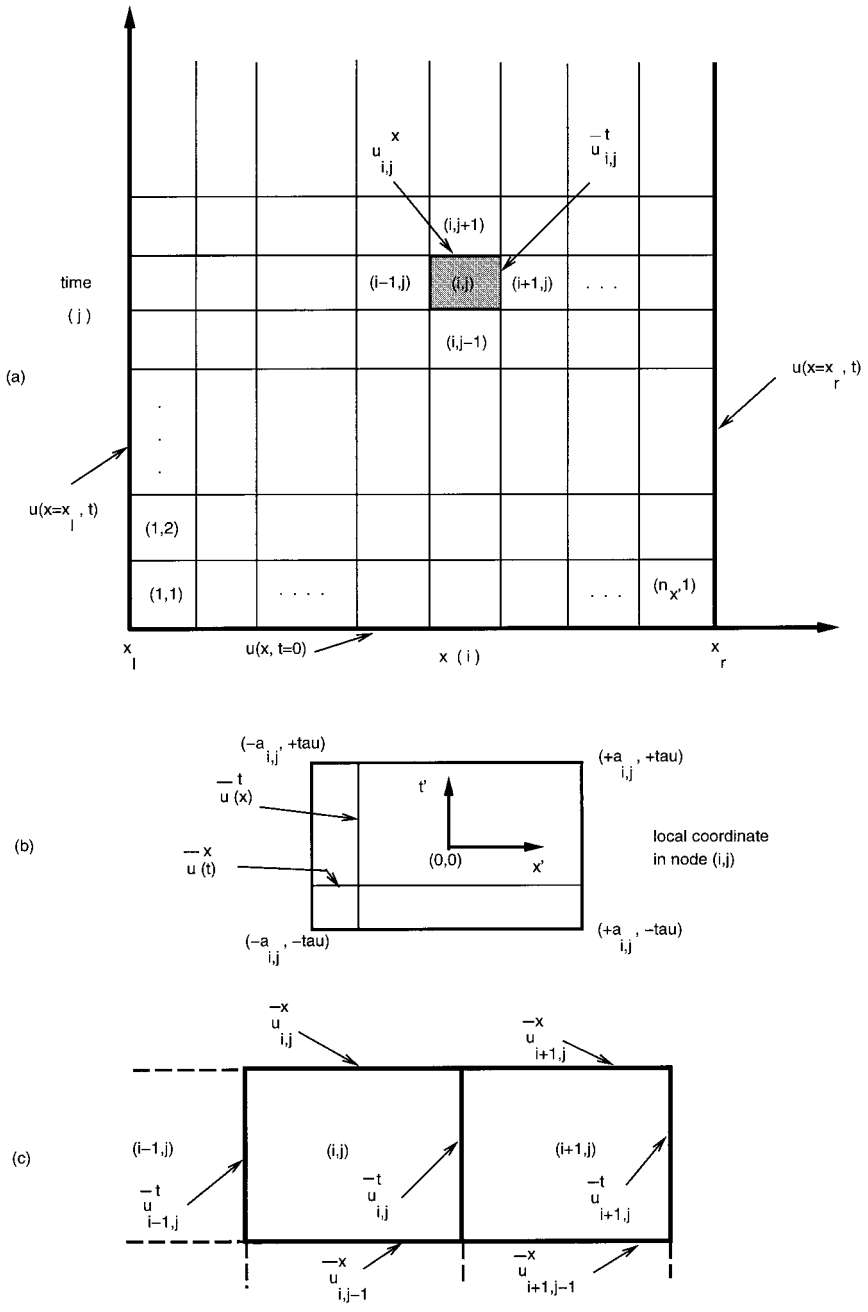

FIG. 1. (a) Schematic diagram of the global (x, t) space, and its division into computational elements or nodes. (b) Local coordinate system within the node (i, j). In the text, primes on x' and t' are dropped for convenience. (c) Averaged quantities on surfaces.

and solve Eq. (9) over the node (i, j). In the conventional NIM, the nonlinear terms are lumped into the pseudo-source term on the right-hand side, and only the linear terms are kept on the left-hand side and solved analytically. Here, we make the approximation that the space-dependent time-averaged velocity $\bar{u}^t(x)$, in the nonlinear convection term only, is actually constant (over the node) equal to the average of the time-averaged $\bar{u}^t$ at $x = +a_{i,j}$ and $x = -a_{i,j}$, i.e., at the left and right (space) boundaries of the node. See Fig. 1(c). The symbol $u^0_{i,j}$ is used to represent the constant velocity. This step then results in a significantly different expression for the solution of $\bar{u}^t(x)$ [compare it with Eq. (A.2)]:

$$\begin{aligned}\bar{u}^t(x) \;=\; & \bar{u}^t(-a_{i,j}) + \frac{d\bar{u}^t(-a_{i,j})}{dx}\left[\frac{e^{[Reu^0_{i,j}(x+a_{i,j})]}-1}{(Reu^0_{i,j})}\right] \\ & + \frac{(Re\bar{S}^{tx}_2)}{(Reu^0_{i,j})}\left[\frac{(e^{[Reu^0_{i,j}(x+a_{i,j})]}-1)}{(Reu^0_{i,j})} - (x+a_{i,j})\right] \end{aligned} \tag{10}$$

when solved in terms of the derivative $\frac{d\,\bar{u}^t}{dx}$ at $x = -a_{i,j}$, and

$$\begin{aligned}\bar{u}^t(x) \;=\; & \bar{u}^t(+a_{i,j}) - \frac{d\bar{u}^t(a_{i,j})}{dx}\left[\frac{1-e^{-[Reu^0_{i,j}(a_{i,j}-x)]}}{(Reu^0_{i,j})}\right] \\ & - \frac{(Re\bar{S}^{tx}_2)}{(Reu^0_{i,j})}\left\{\frac{[1-e^{-Reu^0_{i,j}(a_{i,j}-x)}]}{(Reu^0_{i,j})} - (a_{i,j}-x)\right\} \end{aligned} \tag{11}$$

when solved in terms of the derivative $\frac{d\,\bar{u}^t}{dx}$ at $x = +a_{i,j}$. Rather than a parabolic velocity profile, an exponential variation results within each node, which is similar to the results obtained for the linear, steady-state convection–diffusion equation [1, 2]. The solution is written in terms of $\bar{u}^t_{i,j}(x = +a_{i,j})$ and $\bar{u}^t_{i,j}(x = -a_{i,j})$, which are elements of the vector of discrete unknowns.

Changing i to $(i+1)$ in Eq. (10), evaluating at $x = -a_{i+1,j}$, and solving it for $\frac{d\,\bar{u}^t_{i+1,j}(-a_{i+1,j})}{dx}$ yields the derivative of the velocity on the *right* side of the right boundary of node (i, j):

$$\begin{aligned}\frac{d\bar{u}^t_{i+1,j}(-a_{i+1,j})}{dx} \;=\; & \frac{(Reu^0_{i+1,j})}{[e^{(2Reu^0_{i+1,j}a_{i+1,j})}-1]}\{\bar{u}^t(a_{i+1,j}) - \bar{u}^t(-a_{i+1,j})\} \\ & - Re\bar{S}^{tx}_{2,(i+1,j)}\left\{\frac{1}{(Reu^0_{i+1,j})} - \frac{2a_{i+1,j}}{[e^{(2Reu^0_{i+1,j}a_{i+1,j})}-1]}\right\}. \end{aligned} \tag{12}$$

Equation (11) can be evaluated at $x = +a_{i,j}$ and directly solved for the derivative of the velocity on the *left* side of the right boundary of the node (i, j), $\frac{d\bar{u}^t_{i,j}(+a_{i,j})}{dx}$:

$$\begin{aligned}\frac{d\bar{u}^t_{i,j}(+a_{i,j})}{dx} \;=\; & \frac{(Reu^0_{i,j})}{[1-e^{(-2Reu^0_{i,j}a_{i,j})}]}\{\bar{u}^t(+a_{i,j}) - \bar{u}^t(-a_{i,j})\} \\ & - Re\bar{S}^{tx}_{2,(i,j)}\left\{\frac{1}{(Reu^0_{i,j})} - \frac{2a_{i,j}}{[1-e^{(-2Reu^0_{i,j}a_{i,j})}]}\right\}. \end{aligned} \tag{13}$$

Equating the derivatives on the two sides of the interface between the *i-th* and $(i + 1)$st spatial nodes, and realizing that $\bar{u}^t_{i,j}(+a_{i,j}) = \bar{u}^t_{i+1,j}(-a_{i+1,j})$, we arrive at the three-point scheme that

relates $\bar{u}^t_{i-1,j}$, $\bar{u}^t_{i,j}$, and $\bar{u}^t_{i+1,j}$:

$$\left\{\frac{Reu^0_{i,j}}{[1-e^{-2Reu^0_{i,j}a_{i,j}}]}\right\}\bar{u}^t_{i-1,j}-\left\{\frac{Reu^0_{i,j}}{[1-e^{-2Reu^0_{i,j}a_{i,j}}]}+\frac{Reu^0_{i+1,j}}{[e^{2Reu^0_{i+1,j}a_{i+1,j}}-1]}\right\}\bar{u}^t_{i,j}$$
$$+\left\{\frac{Reu^0_{i+1,j}}{[e^{2Reu^0_{i+1,j}a_{i+1,j}}-1]}\right\}\bar{u}^t_{i+1,j}=Re\bar{S}^{tx}_{2,(i,j)}\left\{\frac{2a_{i,j}}{[1-e^{-2Reu^0_{i,j}a_{i,j}}]}-\frac{1}{Reu^0_{i,j}}\right\}$$
$$+Re\bar{S}^{tx}_{2,(i+1,j)}\left\{\frac{1}{Reu^0_{i+1,j}}-\frac{2a_{i+1,j}}{[e^{2Reu^0_{i+1,j}a_{i+1,j}}-1]}\right\}, \tag{14}$$

where time-averaged velocity in each node is understood to be evaluated at the right spatial (node) boundary ($\bar{u}^t_{i,j}\equiv\bar{u}^t_{i,j}\ (x=+a_{i,j})$).

Four issues must be briefly discussed at this stage of development. First, *two* discrete variables can be associated with each node. For convenience, with node (i,j) we associate the average velocities at the right and top surface of the space-time node, i.e., $\bar{u}^t_{i,j}\ (\equiv\bar{u}^t_{i,j}(+a_{i,j}))$ and $\bar{u}^x_{i,j}\ (\equiv\bar{u}^x_{i,j}(\tau))$ are the unknown discrete variables for the node (i,j). See Fig. 1(c). Second, with Eqs. (8) and (14), for each node (i,j) there are only two equations per node, while the unknowns are four $(\bar{u}^x_{i,j},\bar{u}^t_{i,j},\bar{S}^{xt}_{1,(i,j)},\bar{S}^{tx}_{2,(i,j)})$. So, the additional constraint equations are needed. Third, the equation for the conventional NIM corresponding to Eq. (14) above is the much simpler Eq. (A.3), which only admits at most parabolic velocity profile within each node. Fourth, signs of upwinding are already obvious in Eq. (14).

The additional constraint equations are now developed. The first one is obtained by integrating the original PDE (Burgers equation) over the node (i,j), i.e., operating it with $\frac{1}{4a_{i,j}\tau}\int_{-a_{i,j}}^{+a_{i,j}}\int_{-\tau}^{\tau}dtdx$,

$$\frac{1}{(2\tau)}\int_{-\tau}^{\tau}\frac{d\bar{u}^x(t)}{dt}dt=\frac{1}{(2a_{i,j})}\int_{-a_{i,j}}^{+a_{i,j}}\left[\frac{1}{Re}\frac{d^2\bar{u}^t(x)}{dx^2}-\bar{u}^t(x)\frac{d\bar{u}^t(x)}{dx}\right]dx. \tag{15}$$

Realizing the definitions of $\bar{S}^{xt}_{1,(i,j)}$ and $\bar{S}^{tx}_{2,(i,j)}$ [Eqs. (6) and (9)], the above equation reduces to

$$\bar{S}^{xt}_{1,(i,j)}=\bar{S}^{tx}_{2,(i,j)}. \tag{16}$$

The second constraint equation is obtained by equating $\bar{u}^{xt}_{i,j}$ and $\bar{u}^{tx}_{i,j}$. Operating Eq. (7) with $\frac{1}{2\tau}\int_{-\tau}^{+\tau}dt$ yields $\bar{u}^{xt}_{i,j}$,

$$\bar{u}^{xt}_{i,j}=\bar{u}^x_{i,j-1}+\tau\bar{S}^{xt}_{1,(i,j)}, \tag{17}$$

and operating Eq. (10) with $\frac{1}{2a_{i,j}}\int_{-a_{i,j}}^{+a_{i,j}}dx$ yields $\bar{u}^{tx}_{i,j}$,

$$\bar{u}^{tx}_{i,j}=\left\{\frac{1}{2Reu^0_{i,j}a_{i,j}}-\frac{1}{[e^{2Reu^0_{i,j}a_{i,j}}-1]}\right\}\bar{u}^t_{i,j}$$
$$+\left\{1-\frac{1}{2Reu^0_{i,j}a_{i,j}}+\frac{1}{[e^{2Reu^0_{i,j}a_{i,j}}-1]}\right\}\bar{u}^t_{i-1,j}$$
$$+(Re\bar{S}^{tx}_{2,(i,j)})\left\{\frac{1}{(Reu^0_{i,j})^2}-\frac{a_{i,j}}{(Reu^0_{i,j})}-\frac{2a_{i,j}}{(Reu^0_{i,j})[e^{2Reu^0_{i,j}a_{i,j}}-1]}\right\}. \tag{18}$$

Equating the two yields the last of the constraint equations, which is symbolically written as

$$\bar{u}^{xt}_{i,j} = \bar{u}^{tx}_{i,j}, \tag{19}$$

realizing that explicit expressions for the left-hand side and for the right-hand side are given by Eqs. (17) and (18), respectively.

Equations (8), (14), (16), and (19) are four equations for the four unknowns per node: $\bar{u}^{x}_{i,j}$, $\bar{u}^{t}_{i,j}$, and the pseudo-source terms $\bar{S}^{xt}_{1,(i,j)}$ and $\bar{S}^{tx}_{2,(i,j)}$. Recall that $u^0_{i,j}$ is equal to $(\bar{u}^{t}_{i,j} + \bar{u}^{t}_{i-1,j})/2.0$. In the four-equations and four-unknowns (per node) set described above, it is possible to easily eliminate two of the unknowns, the pseudo-source terms, thus reducing the set to two-equations and two-unknowns per node. We use Eq. (8) to solve for $\bar{S}^{xt}_{1,(i,j)}$, and Eq. (19) to solve for $\bar{S}^{tx}_{2,(i,j)}$. Substituting these expressions for $\bar{S}^{xt}_{1,(i,j)}$ and $\bar{S}^{tx}_{2,(i,j)}$ into Eqs. (14) and (16) yields the final set of two equations for the two discrete variables per node. They are

$$\left(\frac{C_{i,j}-\tau}{\tau}\right)\bar{u}^{x}_{i,j} - \left(\frac{C_{i,j}+\tau}{\tau}\right)\bar{u}^{x}_{i,j-1} + 2A_{i,j}\bar{u}^{t}_{i,j} + 2B_{i,j}\bar{u}^{t}_{i-1,j} = 0 \tag{20}$$

and

$$\begin{aligned} &D_{i,j}\bar{u}^{t}_{i-1,j} + E_{i,j}\bar{u}^{t}_{i,j} + F_{i+1,j}\bar{u}^{t}_{i+1,j} \\ &= \left(\frac{\bar{u}^{x}_{i,j}+\bar{u}^{x}_{i,j-1}}{2(C_{i,j}/Re)}\right)G_{i,j} + \left(\frac{\bar{u}^{x}_{i+1,j}+\bar{u}^{x}_{i+1,j-1}}{2(C_{i+1,j}/Re)}\right)2a_{i+1,j}A_{i+1,j}, \end{aligned} \tag{21}$$

where

$$A_{i,j} \equiv \left\{\frac{1}{2a_{i,j}Reu^0_{i,j}} - H_{i,j}\right\} \tag{22}$$

$$B_{i,j} \equiv 1 - A_{i,j} \tag{23}$$

$$\frac{C_{i,j}}{Re} \equiv \left\{\frac{1}{(Reu^0_{i,j})^2} - \frac{a_{i,j}}{(Reu^0_{i,j})} - \frac{2a_{i,j}H_{i,j}}{(Reu^0_{i,j})}\right\} \tag{24}$$

$$D_{i,j} \equiv Reu^0_{i,j}I_{i,j} + \frac{(1-A_{i,j})}{(C_{i,j}/Re)}G_{i,j} \tag{25}$$

$$E_{i,j} \equiv \frac{A_{i,j}G_{i,j}}{(C_{i,j}/Re)} + \frac{2a_{i+1,j}A_{i+1,j}(1-A_{i+1,j})}{(C_{i+1,j}/Re)} - Reu^0_{i,j}I_{i,j} - Reu^0_{i+1,j}H_{i+1,j} \tag{26}$$

$$F_{i,j} \equiv (Reu^0_{i,j})H_{i,j} + \frac{2A^2_{i,j}a_{i,j}}{(C_{i,j}/Re)} \tag{27}$$

$$G_{i,j} \equiv 2a_{i,j}I_{i,j} - \frac{1}{(Reu^0_{i,j})} \tag{28}$$

$$H_{i,j} \equiv \frac{1}{[e^{2a_{i,j}Reu^0_{i,j}} - 1]} \tag{29}$$

$$I_{i,j} \equiv \frac{1}{[1 - e^{-2a_{i,j}Reu^0_{i,j}}]}. \tag{30}$$

Corresponding equations for the conventional NIM are Eqs. (A.8) and (A.9). The template for the modified NIM is the same as that for the conventional NIM. Equation (20) can be viewed as the equation for the space-averaged velocity for node (i,j), $\bar{u}^x_{i,j}$ [in terms of average velocities on the other three surfaces—$\bar{u}^x_{i,j-1}$, $\bar{u}^t_{i,j}$, and $\bar{u}^t_{i-1,j}$—of the node (i,j)]. Equation (21) can then be used to determine the time-averaged velocity $\bar{u}^t_{i,j}$ in terms of $\bar{u}^t_{i-1,j}$, $\bar{u}^t_{i+1,j}$, $\bar{u}^x_{i,j}$, $\bar{u}^x_{i,j-1}$, $\bar{u}^x_{i+1,j}$, and $\bar{u}^x_{i+1,j-1}$.

Two rather important observations can be made. First, the template and the unknown discrete variables in the conventional NIM and the modified NIM are the same. The set of final discrete equations in both cases are nonlinear, and, hence, the solution scheme used for one can be used for the other. Second, the new scheme has the same characteristic inherent upwinding that resulted in the NIM solution of the linear, steady-state convection–diffusion equation; the magnitude of the coefficients of the two neighboring time-averaged velocities, $\bar{u}^t_{i-1,j}$ and $\bar{u}^t_{i+1,j}$, needed to calculate the time-averaged velocity $\bar{u}^t_{i,j}$ depend upon the flow direction in the two neighboring nodes. For high Reynolds number and flow from left to right, $\bar{u}^t_{i-1,j}$ contributes more to $\bar{u}^t_{i,j}$ than $\bar{u}^t_{i+1,j}$. In the limit of no diffusion, the influence of $\bar{u}^t_{i+1,j}$ on $\bar{u}^t_{i,j}$ completely disappears. As the new formalism is a generalization of the conventional NIM, the final equations [Eqs. (20) and (21)] reduce to those of the conventional NIM [Eqs. (A.8) and (A.9)] in the limit of small cell Reynolds number $(2auRe)$. This is shown explicitly in Appendix B.

Reference 4 presents a block iterative scheme for the solution of the set of discrete equations. We use the simple iterative scheme in which, at each time step starting from the left boundary, $\bar{u}^t_{i,j}$ and $\bar{u}^x_{i,j}$ are evaluated for each node using Eq. (21) and Eq. (20), respectively, for i from 1 to n_x (of course, $\bar{u}^t_{n_x,j}$ is not evaluated because that is the boundary condition). The process is repeated until convergence is achieved.

An important feature of the nodal integral methods is their ability to yield expressions for the distribution of the dependent variables, averaged in all but one direction within the nodes, that are self-consistent with the converged value of the discrete variables at the node boundaries. For Burgers equation, an expression for $\bar{u}^t_{i,j}(x)$ can be obtained by simply substituting Eq. (13) into Eq. (11):

$$\begin{aligned}\bar{u}^t(x) \;=\; & \bar{u}^t(+a_{i,j}) - \left\{ \frac{(Reu^0_{i,j})}{[1-e^{(-2Reu^0_{i,j}a_{i,j})}]}\{\bar{u}^t(+a_{i,j}) - \bar{u}^t(-a_{i,j})\} \right. \\ & \left. - Re\bar{S}^{tx}_{2,(i,j)}\left[\frac{1}{(Reu^0_{i,j})} - \frac{2a_{i,j}}{[1-e^{(-2Reu^0_{i,j}a_{i,j})}]}\right]\right\} \\ & \times \left[\frac{1-e^{[Reu^0_{i,j}(a_{i,j}-x)]}}{(Reu^0_{i,j})}\right] - \frac{(Re\bar{S}^{tx}_2)}{(Reu^0_{i,j})}\left\{\frac{[1-e^{-[Reu^0_{i,j}(a_{i,j}-x)]}]}{(Reu^0_{i,j})} - (a_{i,j}-x)\right\}. \end{aligned} \tag{31}$$

This last equation is in terms of $\bar{u}^t(a_{i,j})$, $\bar{u}^t(-a_{i,j})$, $\bar{u}^0_{i,j}(=(\bar{u}^t_{i,j}+\bar{u}^t_{i-1,j})/2)$, and $\bar{S}^{tx}_{2,(i,j)}$. Since $\bar{S}^{tx}_{2,(i,j)} = \bar{S}^{xt}_{1,(i,j)}$ [Eq. (16)] and $\bar{S}^{xt}_{1,(i,j)}$ is given in Eq. (8) in terms of $\bar{u}^x_{i,j}$ and $\bar{u}^x_{i,j-1}$, all the quantities in Eq. (31) are known and the node interior solution can be constructed. For large nodes with significant nonlinear variation within the nodes, this reconstruction can improve the accuracy of the results. The important point to note here is that this reconstruction is carried out *after* the discrete variables are solved by whatever technique is used. A useful application of the ability to determine the node interior distribution will be shown in the next section for a time-dependent problem with periodic initial condition.

IV. NUMERICAL EXAMPLES

The steady-state and time-dependent Burgers equations are solved to demonstrate the properties of the modified NIM. This section is divided into three parts. First we solve the steady-state Burgers equation and numerically study the convergence properties of the modified NIM. Next, the numerical scheme developed here is applied to two well known time-dependent problems with known exact solutions that have been frequently used in the past to compare numerical schemes [4, 13, 15–17].

The discrete variables in the NIMs are not values of dependent variables at specific points of space and time, rather these methods yield dependent variables averaged over *surfaces.* In steady-state problems, surfaces are the conventional node surfaces, say a surface in yz plane at a specific x value. The averaging for time-dependent problems could be either over one or more spatial direction(s), or it could be even over a time interval and one or more space dimensions of the node. The discrete variables for a one-dimensional time-dependent problem (Burgers equation) are dependent variables averaged over the width of the spatial node evaluated at specific value of time, and dependent variables averaged over the *height* of the node in the time direction evaluated at specific values for the spatial coordinate (see Fig. 1). Error analysis for the NIMs requires that the exact solution used as reference should also be averaged over appropriate node surfaces. For one-dimensional Burgers equation, by convention, associated with each node (i, j) are two discrete variables; $u(x, t)$ averaged over x (of that node) evaluated at the end of the time step $\bar{u}^x_{i,j}$ (top surface of the node); and $u(x, t)$ averaged over the time interval Δt evaluated at the right edge of the node, $\bar{u}^t_{i,j}$. (See Fig. 1.) Both quantities can be plotted as a function of x for different values of t. Or the evolution of either one of them for a given node can be plotted vs. time. Because $\bar{u}^x_{i,j}$ are values averaged over the width of the node, they are better plotted at the node center, hence making a direct comparison with finite difference schemes a little difficult. Though $\bar{u}^t_{i,j}$ are velocity values at node edges, which may correspond to finite difference grid points, a direct comparison between the results of the finite difference schemes and $\bar{u}^t_{i,j}$ of the NIM is still problematic, since the result of the NIM $(\bar{u}^t_{i,j})$ are values averaged over a time interval $\Delta t = 2\tau$, where as the result of the finite difference schemes are values at a given time t. Visual qualitative comparison can nevertheless be easily made by plotting the results on the same graph. For quantitative comparison we use the exact solution as reference, and report root mean square (RMS) errors for both the finite difference scheme and the NIM, where the exact solutions are appropriately determined for each case: point values for finite difference scheme and time- or space-averaged values for NIM.

A. Steady-State Problem

Steady-state problems can be solved using both a steady-state formulation of the Burgers equation and using the time-dependent formulation. The steady-state formulation was also coded and tested. Both the time-dependent formulation and the steady-state formulation yielded the same results for the steady-state problem.

We make use of the well known exact solution of the Burgers equation:

$$u(x) = -\frac{2}{Re}\tanh(x) \qquad 0 \le x \le 1, \tag{32}$$

where

$$u(0) = 0 \quad \text{and} \quad u(1) = -\frac{2}{Re}\tanh(1), \tag{33}$$

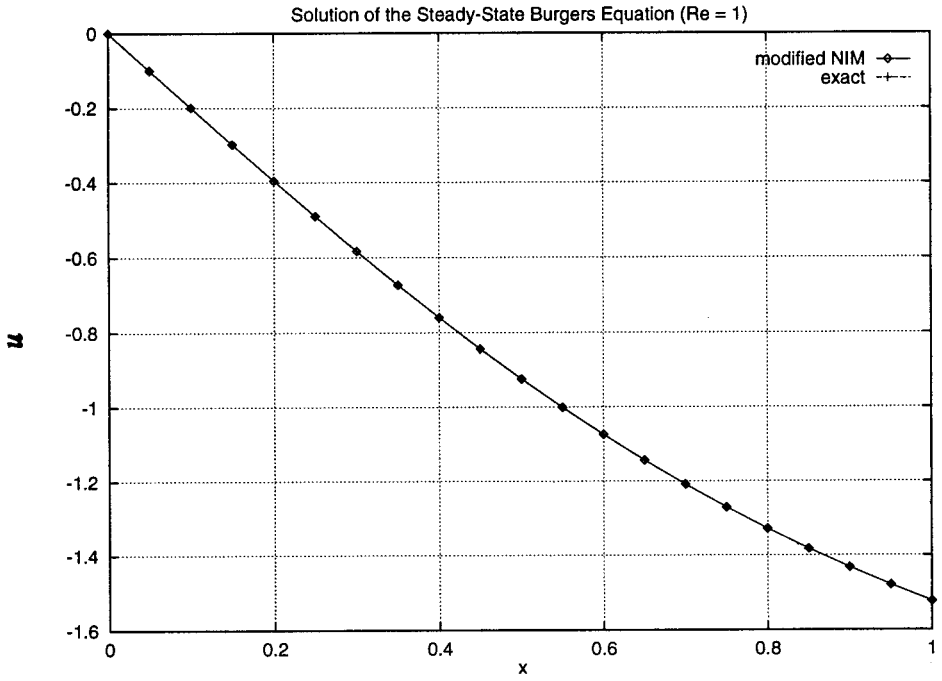

FIG. 2. Solution of the steady-state Burgers equation using MNIM, and the exact solution.

and solve the steady-state formulation of the modified nodal integral method (MNIM) for various Reynolds numbers and on various node sizes. Appropriate boundary conditions at the left and right boundaries $x = x_\ell = 0$ and $x = x_r = 1$, are specified.

Shown in Fig. 2 are the exact solution and the solution obtained using the MNIM for $Re = 1$. Note that, for steady-state problems in one space dimension, NIM yields point values at node boundaries, and, hence, its comparison with the exact solution is straightforward. The root mean square error (RMS), defined by

$$RMS = \frac{1}{N^{1/2}} \sqrt{\sum_{i=1}^{N} (u_i - u_{i,exact})^2}, \tag{34}$$

where N is the number of unknown discrete variables, for the solution of the steady-state problem shown in Fig. 2 is 0.3989×10^{-4}. Since the pseudo-source term was truncated at the zeroth order before solving the transverse integrated equations, the method is theoretically expected to be of second order [9, 10, 4]. To test the spatial convergence rate of the numerical scheme developed here, the steady-state problem for $Re = 1$ was solved on various mesh sizes. The RMS error is plotted vs. node size $(2a)$ in Fig. 3 and tabulated in Table I. The slope in Fig. 3 is approximately 2, implying that the modified NIM is $O(a^2)$. Note that the conventional NIM developed for Burgers equation is also O(a^2) [4].

B. Time-Dependent Problem No. 1

To test the numerical scheme for time-dependent problems, especially at high Reynolds numbers, the scheme is applied to the well-known propagating shock wave problem, which has an exact

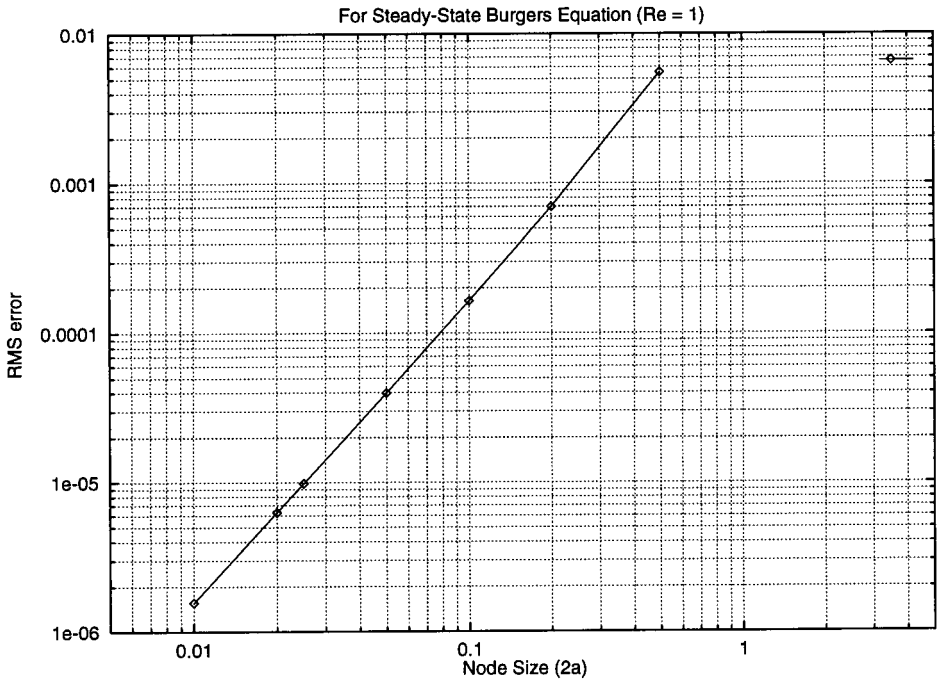

FIG. 3. RMS error in the solution of the steady-state equation plotted vs. node size $2a$.

solution. Numerical schemes' ability to accurately track the shock front in this problem without introducing wiggles is important. Equation (1) is solved over $x \in [-2, 2]$ with the following initial and boundary conditions:

$$u(x < 0, 0) = 1 \quad \text{and} \quad u(x > 0, 0) = 0 \tag{35}$$

$$u(x_\ell, t) = 1 \quad \text{and} \quad u(x_r, t) = 0, \tag{36}$$

where $x_\ell = -2$ and $x_r = +2$. Exact solution of the above problem [15] is given by

$$u_{exact}(x, t) = \int_{-\infty}^{\infty} [(x - \xi)/t] e^{-0.5ReG} \Big/ \int_{-\infty}^{\infty} e^{-0.5ReG}\, d\xi, \tag{37}$$

TABLE I. RMS error vs. node size for steady-state Burgers equation ($Re = 1$).

$2a(\Delta x)$	RMS error
0.500	0.5539×10^{-2}
0.200	0.6957×10^{-3}
0.100	0.1639×10^{-3}
0.050	0.3989×10^{-4}
0.025	0.9844×10^{-5}
0.020	0.6284×10^{-5}
0.010	0.1563×10^{-5}

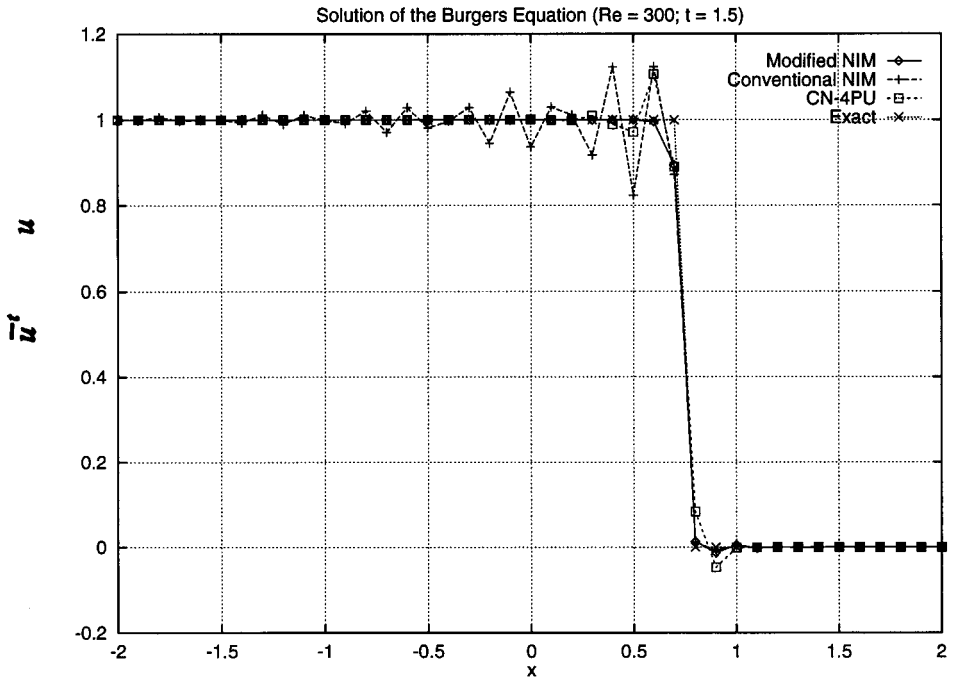

FIG. 4. A general comparison for the standard propagating shock wave problem among the exact solution, modified NIM, conventional NIM, and CN-4PU for $Re = 300$, $t = 1.5$, $2\tau = 0.05$. Values plotted for the exact solution and for CN-4PU scheme are values at $t = 1.5$. Values plotted for MNIM and CNIM are the quantities averaged over the last time interval, $\bar{u}^t_{i,j}$.

where

$$G(\xi; x, t) = \int_0^{\xi} u(\xi', 0)\, d\xi' + \frac{0.5(x - \xi)^2}{t}. \tag{38}$$

For a general comparison between the conventional nodal integral method (CNIM), modified nodal integral method (MNIM), and one of the finite difference schemes, the Burgers equation is solved for $Re = 300$ with 40 nodes in $-2 < x < 2(\Delta x = 2a = 0.1, \Delta t = 2\tau = 0.05)$. The finite difference scheme chosen here is the Crank–Nicolson, four-point upwind (CN-4PU) [15]. Solution of the Burgers equation for the three numerical schemes and the exact solution are plotted in Fig. 4. Note that while the exact solution and the solution of the finite difference scheme are the u values at $t = t_f = 1.5$, solution of the CNIM and MNIM are actually average of the velocities from $t = t_f - 2\tau$ to $t = t_f$. In this particular case, they are averaged from $t = 1.45$ to $t = 1.50$. Though all three schemes rather accurately track the wave front, the MNIM shows the least oscillations—so typical in such solutions—near the wave front.

A quantitative comparison of, say, RMS errors between these schemes and the exact solution requires not only the exact solution at discrete space and time coordinates as given by Eqs. (37) and (38) (for the finite difference scheme), but also requires the solution averaged over space, and solution averaged over time intervals for the nodal methods. Hence, to facilitate this comparison a slightly modified problem with time-dependent boundary conditions is solved. The solution of this modified propagating shock wave problem has a particularly simple form. The initial and

boundary conditions for the modified problem [14, 4] are

$$u(x,0) = \frac{b}{Re}\left\{1 - \tanh\left(\frac{bx}{2}\right)\right\} \tag{39}$$

$$u(-2,t) = \frac{b}{Re}\left\{1 - \tanh\left[-b - \frac{b^2}{2Re}t\right]\right\} \tag{40}$$

$$u(+2,t) = \frac{b}{Re}\left\{1 - \tanh\left[b - \frac{b^2}{2Re}t\right]\right\}, \tag{41}$$

and the solution is

$$u(x,t) = \frac{b}{Re}\left\{1 - \tanh\left[\frac{bx}{2} - \frac{b^2}{2Re}t\right]\right\}. \tag{42}$$

With arbitrary parameter b chosen as $b = Re/2$ [4], the solution becomes

$$u(x,t) = \frac{1}{2}\left\{1 - \tanh\left[\frac{Rex}{4} - \frac{Ret}{8}\right]\right\}. \tag{43}$$

By allowing the boundary condition to change with time, a simpler closed form solution is obtained, which has essentially all the characteristics of the solution given by Eqs. (37) and (38). Moreover, the space and time-averaging of the exact solution of the modified problem is significantly easier. Expressions for time-averaged (over 2τ) and space-averaged (over $2a$) values for u_{exact}, $\bar{u}^t(x)$, and $\bar{u}^x(t)$ are given in Appendix C for reference.

Figures 5(a) and 5(b) show the results of the MNIM for the problem given by Eqs. (1), (39), (40), and (41) for $Re = 300$ and $t = 1.5$. The domain is divided into 100 nodes, and $\Delta t = 0.05$. The velocity averaged over the last time interval $\bar{u}^t$ is plotted in Fig. 5(a), and the velocity averaged over each node's spatial dimension is plotted (at the center of the node) in Fig. 5(b). Clearly, the MNIM can track the wave front very accurately even at such high Reynolds number with negligible oscillations and without the introduction of any artificial dissipation. The error in space-averaged quantities is less than those in time-averaged quantities, with RMS error in $\bar{u}^t$, $\bar{u}^x$, and for both $\bar{u}^t$ and $\bar{u}^x$ being $0.1002 \times 10^{-1}, 0.1560 \times 10^{-2}$, and 0.7150×10^{-2}, respectively.

To determine the error introduced due to time discretization, we simply solve the modified propagating shock wave problem with a large number of spatial nodes (to have minimum error due to space discretization) for one time-step for several values of $\Delta t (= 2\tau)$. RMS error for each Δt is calculated and plotted against the time step in Fig. 6 and tabulated in Table II. The method is clearly $0(\Delta t^2)$, though, as is well known for such tests, at small values of Δt the order drops below 2, because the errors introduced due to spatial discretization at small time-steps start to contribute to the overall error.

Results of a quantitative comparison between MNIM, CNIM, and CN-4PU scheme are presented in Figs. 7–10 and in Table III. Calculations are carried out with 20 spatial nodes and a rather large time-step (2τ) of 0.1 for two different Reynolds numbers. Figure 7(a) shows the results of CNIM and MNIM solution for $Re = 50$ and $t = 1.0$. Space-averaged $\bar{u}^x_{i,j}$ are plotted at the center of each node. The exact solution appropriately averaged over each node is also plotted. Corresponding comparison between CN-4PU scheme and the exact solution–values at grid points in this case–are plotted in Fig. 7(b). To determine if these numerical schemes have characteristically different accumulation of errors at large time, the above calculations are repeated for $t = 3.0$, and the results are plotted in Figs. 8(a) and 8(b). RMS errors for both of these calculations are

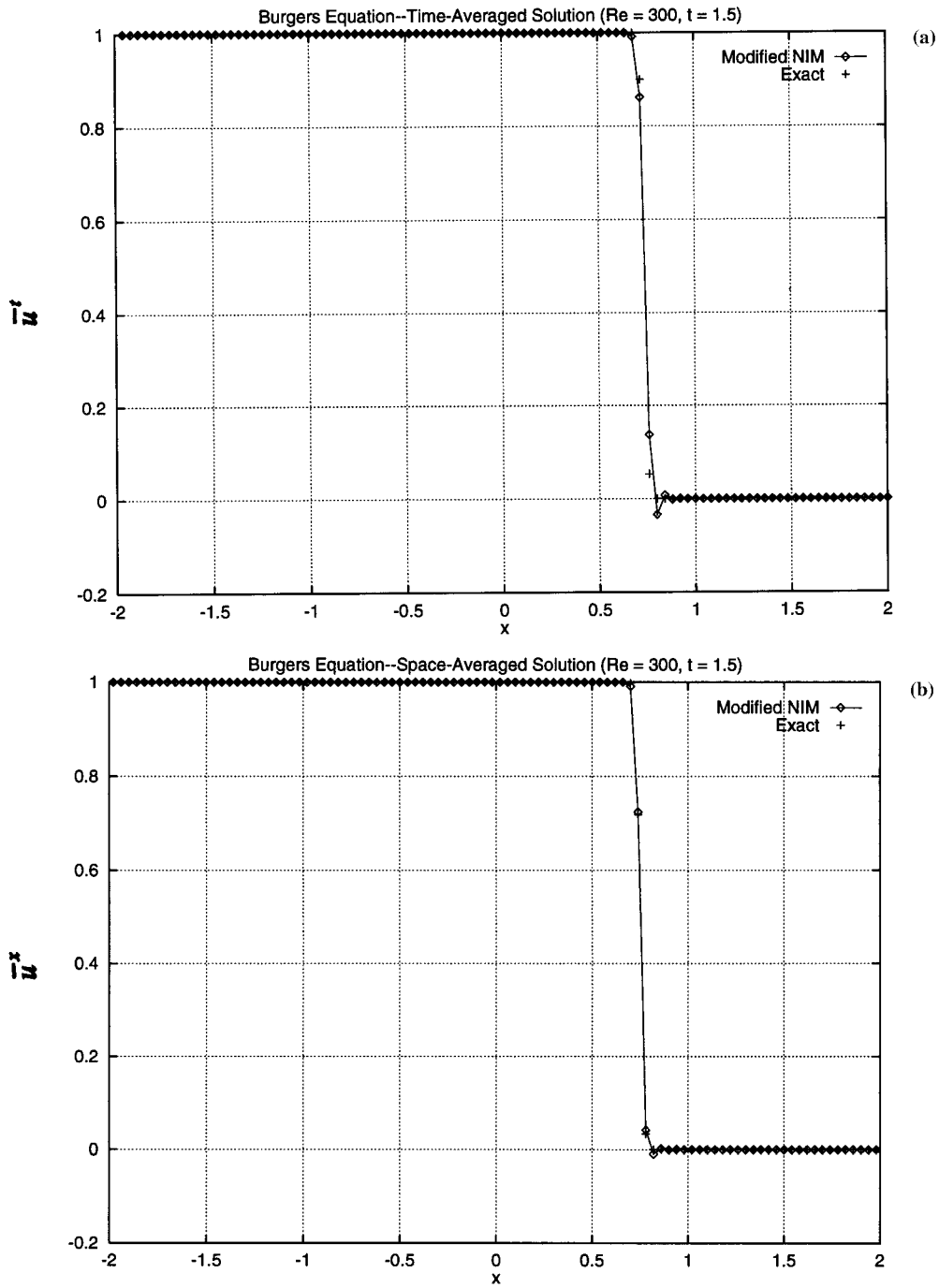

FIG. 5. A general comparison between the solution of the modified NIM and the exact solution for the modified propagating shock wave problem ($Re = 300$, 100 nodes, $2\tau = 0.05$, $t = 1.5$). a) $\bar{u}^x$ vs. exact $\bar{u}^x$, b) $\bar{u}^t$ vs. exact $\bar{u}^t$. RMS error in $\bar{u}^x$ values is 0.1562×10^{-2}, in $\bar{u}^t$ values is 0.1002×10^{-1}, and, in both $\bar{u}^x$ and $\bar{u}^t$ values, is 0.7155×10^{-2}.

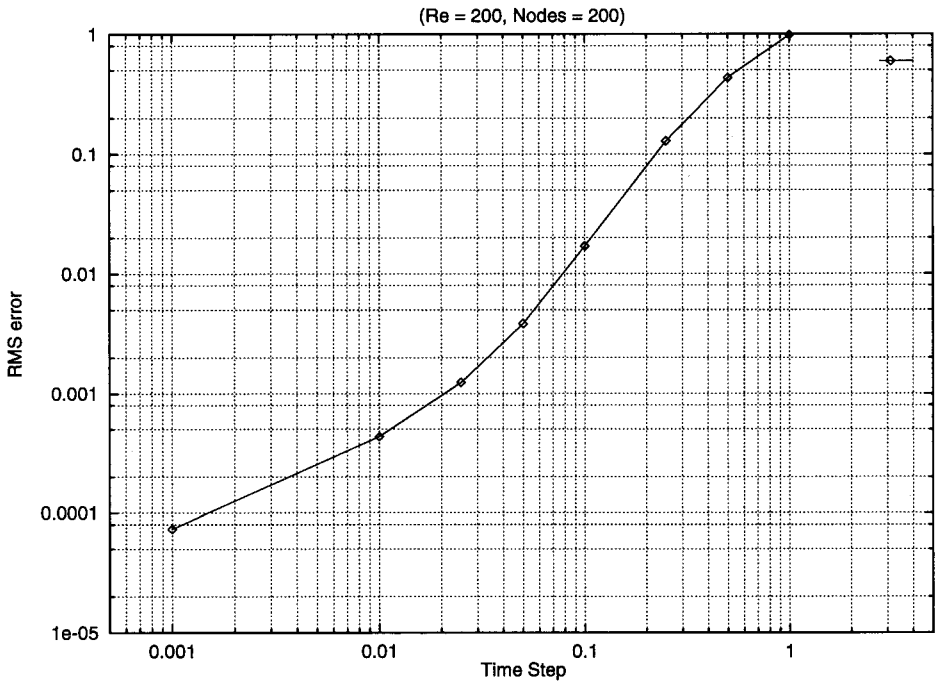

FIG. 6. RMS error vs. time step for the modified NIM after one time step ($Re = 200$, 200 nodes).

tabulated in Table III. The difference among these schemes at the low Reynolds number of 50 is rather small. Though all can track the wave front quite accurately, both CNIM and CN-4PU schemes lead to spurious oscillations near the wave front.

To assess the numerical scheme at relatively large Reynolds number, the modified propagating shock wave problem is solved for the same parameter values as in Figs. (7) and (8), and for a Reynolds number of 100. Corresponding results are plotted in Figs. 9(a), 9(b), 10(a), and 10(b), and tabulated in Table III. The modified NIM at this large value of Reynolds number is clearly superior to both CNIM and CN-4PU schemes. The RMS error for MNIM is smaller than the RMS error for CN-4PU scheme by a factor of at least two, and smaller by a factor of at least three when compared with the corresponding RMS error for the CNIM. While the ability of the CN-4PU scheme to closely track the wave front even at large time $(t = 3)$ is quite impressive [Fig. 10(b)],

TABLE II. RMS error vs. time step $2\tau(\Delta t)$, for one time step (200 nodes; $Re = 1$).

$2\tau(\Delta t)$	RMS error
1.000	0.9810×10^{0}
0.500	0.4330×10^{0}
0.250	0.1285×10^{0}
0.100	0.1698×10^{-1}
0.050	0.3826×10^{-2}
0.025	0.1244×10^{-2}
0.010	0.4350×10^{-3}
0.001	0.7357×10^{-4}

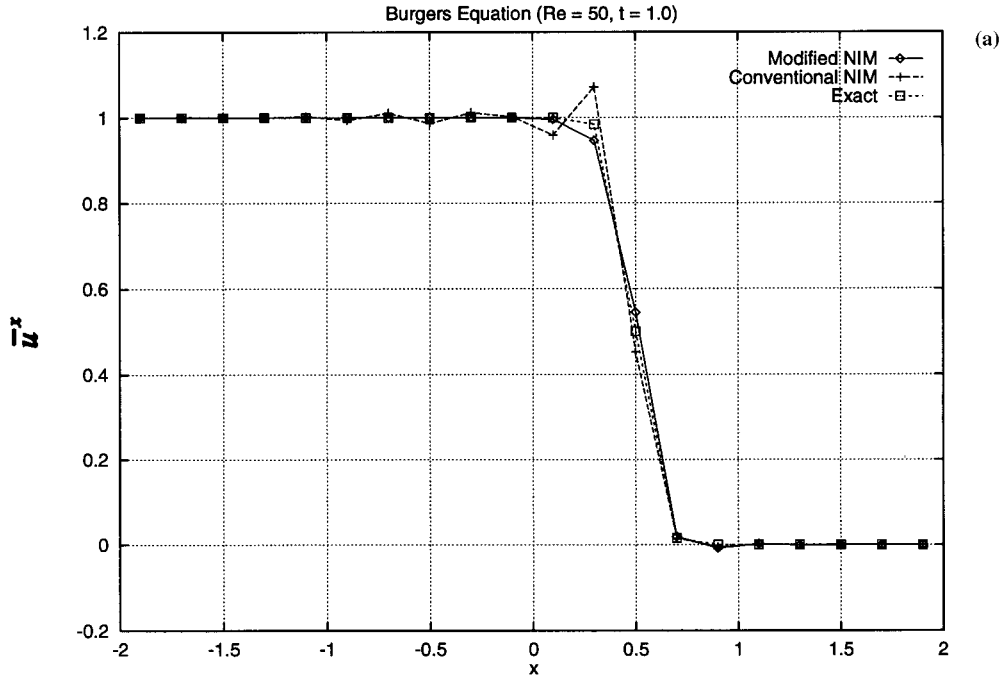

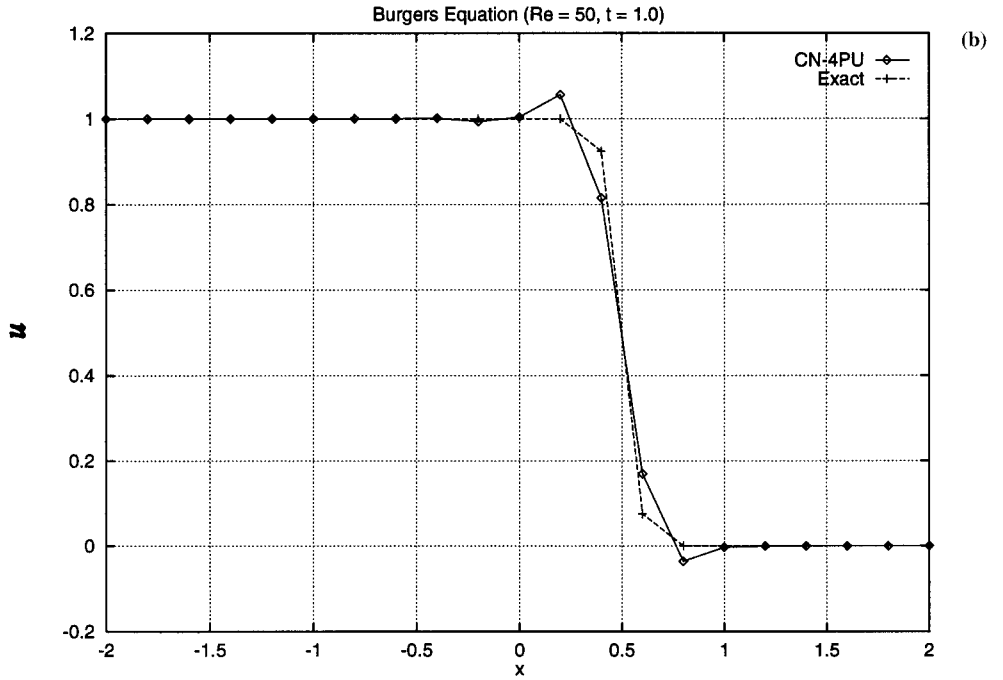

FIG. 7. (a) Comparison of the solution ($\bar{u}^x$) of the modified propagating shock wave problem obtained using conventional NIM and modified NIM with the exact solution for $Re = 50$, $t = 1.0$, and $2\tau = 0.01$. (b) Comparison between solution obtained using CN-4PU scheme with the exact solution.

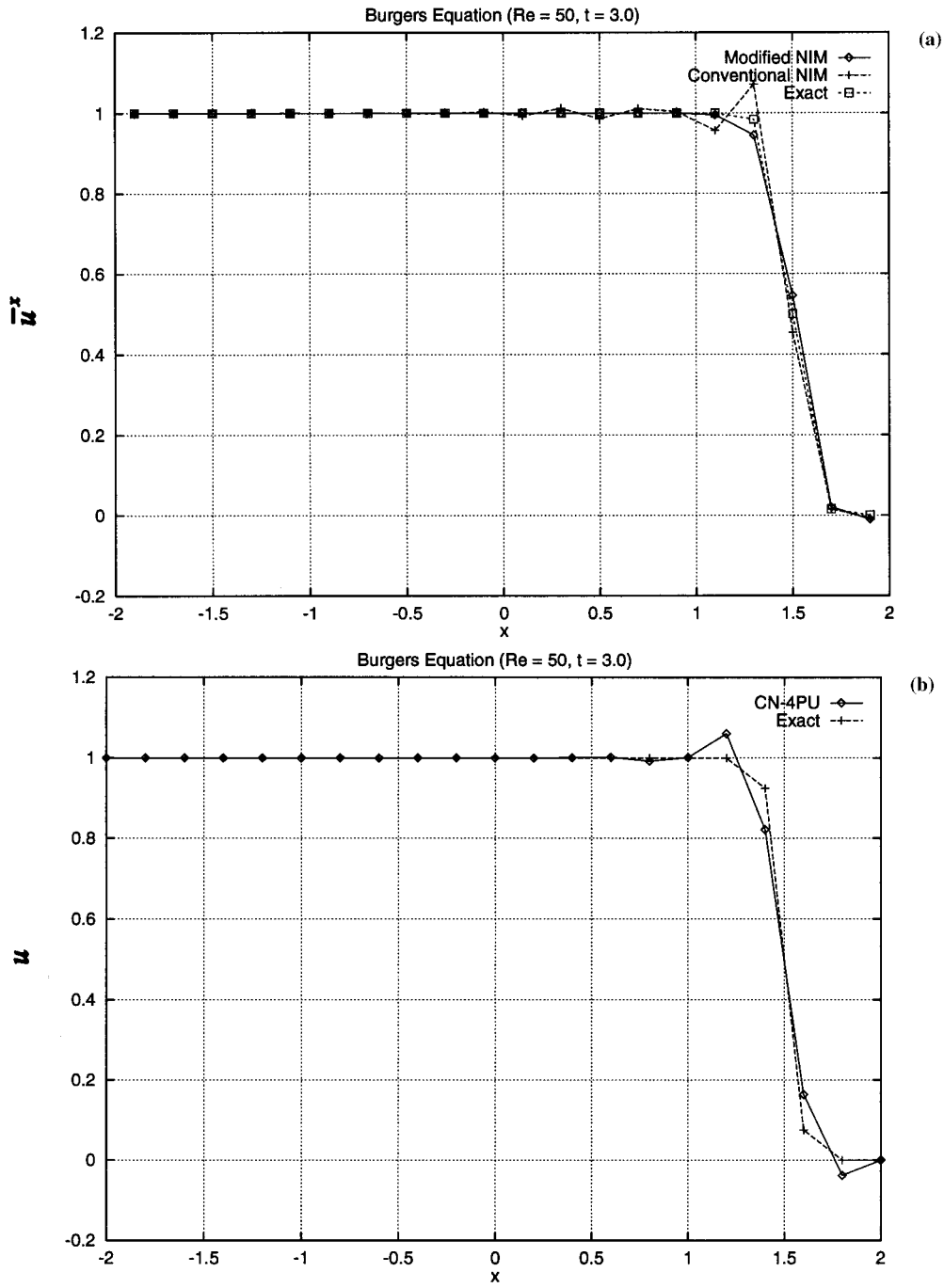

FIG. 8. See caption for Fig. 7 ($t = 3.0$).

it is accompanied with wiggles soon before and after the front. The MNIM, on the other hand, shows minimum oscillations and can still track the wave front very accurately.

The RMS error values tabulated in Table III are given for the RMS error in $\bar{u}^x$, RMS error

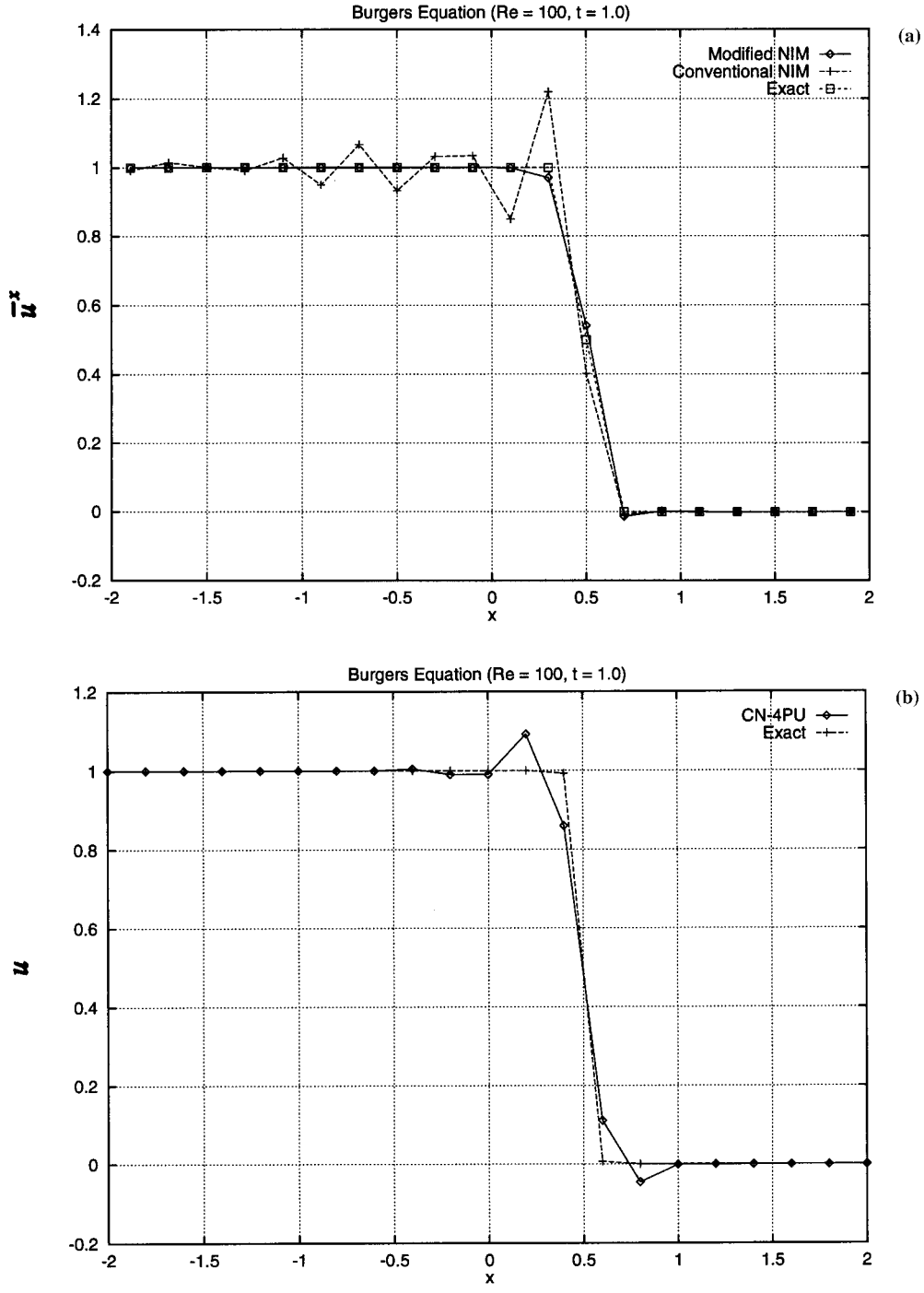

FIG. 9. See caption for Fig. 7 ($Re = 100$, $t = 1.0$, $2\tau = 0.01$).

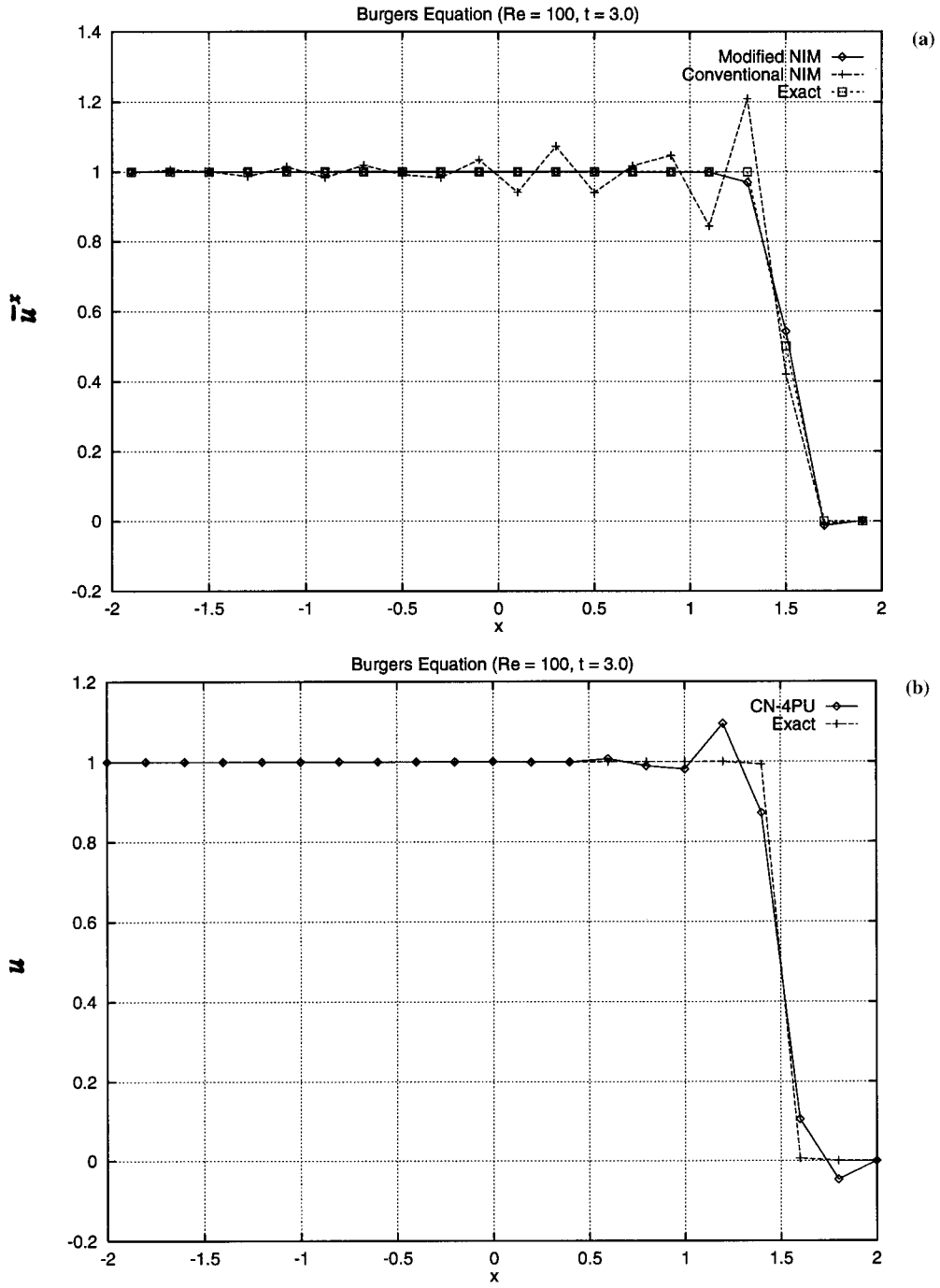

FIG. 10. See caption for Fig. 7 ($Re = 100$, $t = 3.0$, $2\tau = 0.01$).

in $\bar{u}^t$, and RMS error in both $\bar{u}^x$ and $\bar{u}^t$ values. For reference, $\bar{u}^t$ values are plotted in Fig. 11 for $Re = 100$ at $t = 3.0$. This should be compared with Figs. 10(a) and 10(b). Though not as accurate as its sister $\bar{u}^x$ values (MNIM) shown in Fig. 10(a), RMS error in $\bar{u}^t$ values (MNIM) is still less than the RMS error from CN-4PU scheme.

TABLE III. RMS errors for MNIM, CNIM, and CN-4PU (20 nodes; $\Delta t = 0.1$).

		Re = 50		Re = 100	
		$t = 1.0$	$t = 3.0$	$t = 1.0$	$t = 3.0$
CN-4PU		0.3652×10^{-1}	0.3524×10^{-1}	0.4546×10^{-1}	0.4367×10^{-1}
CNIM		0.3091×10^{-1}	0.3068×10^{-1}	0.6558×10^{-1}	0.6376×10^{-1}
MNIM	$\bar{u}^t$	0.2721×10^{-1}	0.2775×10^{-1}	0.2666×10^{-1}	0.2678×10^{-1}
	$\bar{u}^x$	0.1338×10^{-1}	0.1382×10^{-1}	0.1172×10^{-1}	0.1185×10^{-1}
	$\bar{u}^x$ and $\bar{u}^t$	0.2127×10^{-1}	0.2175×10^{-1}	0.2041×10^{-1}	0.2053×10^{-1}

To demonstrate the node interior reconstruction capability of the NIMs, the problem is solved with a large Reynolds number of 300 and small number of nodes (10). Solution of the MNIM for this problem at $t = 1$ (with $2\tau = \Delta t = 0.025$) is shown in Fig. 12, where $\bar{u}^t$ values at nine interior $x =$ *constant* surfaces are plotted and connected by straight lines. Also shown is the reconstructed node interior solution within each node, and the exact $\bar{u}^t(x)$ (see Appendix C). Recall that an expression for the node interior solution for the MNIM was obtained during the development of the MNIM. The fact that coupling scheme between neighboring nodes was obtained by requiring that the derivative at node interfaces be continuous leads to a continuous and differentiable reconstructed solution over the entire domain. While reconstructed solutions within all other nodes are quite uneventful, node number 8 $(0.8 \leq x \leq 1.2)$ shows how the reconstructed solution can be much more accurate when compared with a straight-line-connected solution. Additional information that can be obtained from the node interior reconstructed solu-

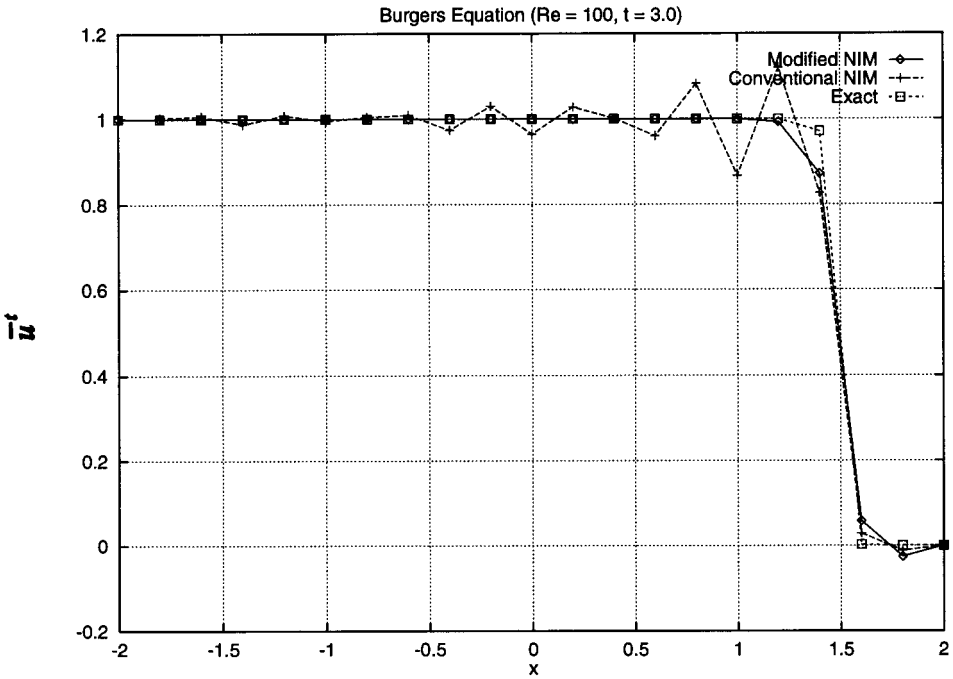

FIG. 11. Comparison of the time-averaged velocities ($\bar{u}^t$) calculated using conventional NIM and modified NIM with the corresponding exact solution (for parameters used in Fig. 10).

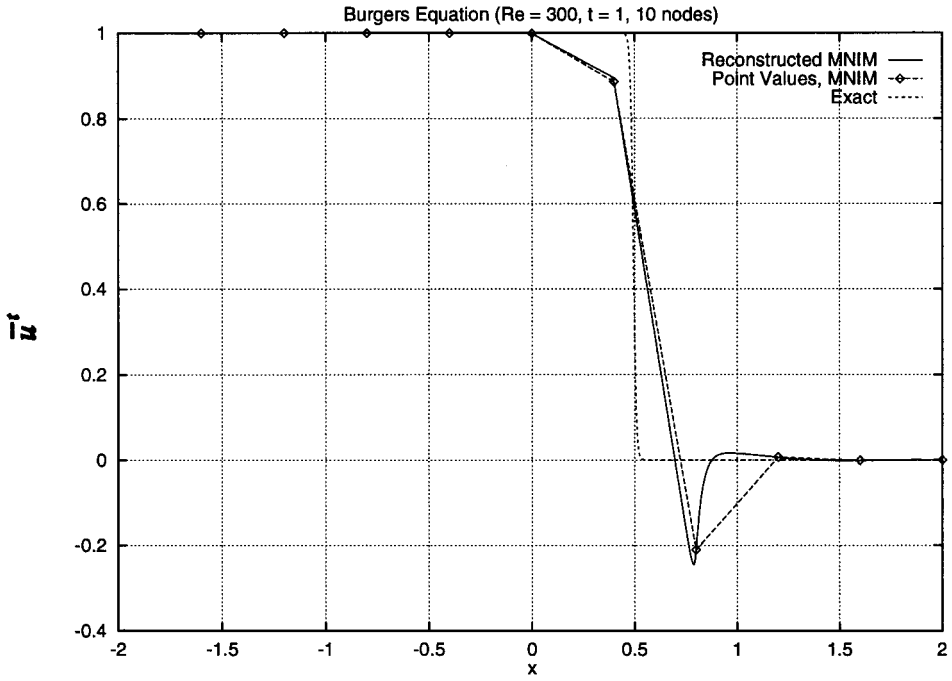

FIG. 12. Solution obtained using the modified NIM (point values), and the solution after node interior reconstruction.

tion is demonstrated again—and much more strongly than the propagating shock wave problem permitted—in the second time-dependent problem that follows.

C. Time-Dependent Problem No. 2

To further test the numerical scheme for time-dependent problems and to demonstrate additional characteristics of the MNIM, we solve the well known problem with periodic initial condition [14, 16, 17]:

$$u(x,0) = -\sin(\pi x) \qquad -1 \le x \le 1 \tag{44}$$

and boundary conditions

$$u(\pm 1, t) = 0. \tag{45}$$

As is well known, the exact analytical solution of this problem [14, 16] is *numerically untractable* for small t and large Reynolds numbers [16]. Moreover, as discussed earlier, averaged quantities are calculated by the NIMs, and they should be compared with appropriately averaged exact solutions. We do not make any attempt to calculate the exact solution averaged over appropriate time or space intervals, and, hence, do not compare the RMS errors for different schemes. As in Ref. 16, we determine the maximum of the $|\frac{\partial u}{\partial x}(x=0)|$ and the time $t_{\max}$ that the maximum derivative is reached. The value of the derivative at the origin is rather sensitive and a very good measure of the numerical scheme's accuracy [16]. Basdevant et al. [16] discuss this problem in detail and solve it using several techniques for $Re = 100\pi$. Fourier spectral method, Chebyshev spectral methods, and finite difference method were used to solve the Burgers equation and the

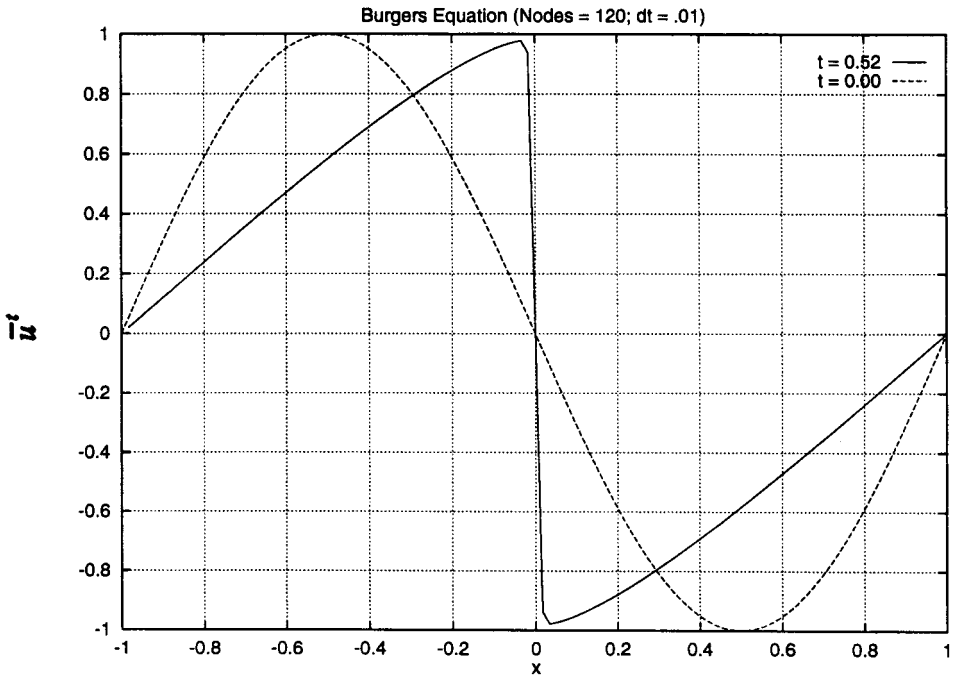

FIG. 13. Solution of the Burgers equation ($\bar{u}^t$) with periodic initial condition over $[-1, 1]$ using modified NIM, at $t = 0.52$ with $Re = 100\pi$, 120 nodes, and $2\tau = 0.01$.

results were compared. The maximum of the absolute value of the derivative reached at the origin and the corresponding time were tabulated for each method. The exact values for these two quantities are 152.00516 and 0.5105, respectively. The time-steps used ranged from $10^{-2}/\pi$ to $5 \times 10^{-4}/\pi$, while the treatment of space *discretization* obviously varied from one method to another. It is quite obvious that rather fine discretization in space is required by all methods to avoid oscillations, and to accurately predict the derivative at the center. Some of the methods required the introduction of artificial viscosity to dampen the oscillations. It was concluded that spectral schemes offered the best accuracy, especially if coordinate transformation (to accumulate grid points in the region of steep gradient) is used to resolve the narrow region of large variation of the dependent variable [16].

As discussed in Section III, and in Section IVA in the context of the propagating shock wave problem, the ability of the NIM to reconstruct the node interior solution can often considerably reduce the node size required. The maximum of the absolute value of the derivative in the current problem can be evaluated by reconstructing the node interior solution in the nodes on either side of $x = 0$—and both sides will necessarily yield the same derivative. The derivative can also be calculated by applying the finite difference formula on two neighboring u values in the node on either side of $x = 0$. This will be referred to as the finite difference approach. To demonstrate the additional accuracy that results when reconstruction is employed, the values of the maximum derivative as calculated using the finite difference approach, and as calculated using the reconstruction approach will both be reported.

Figure 13 shows the solution of the above problem obtained using the modified NIM with 120 nodes at $t = 0.52$. (Reynolds number for all these calculations is 100π.) Shown are the $\bar{u}^t$ values connected by straight lines. Maximum of the absolute value of the derivative at $x = 0$

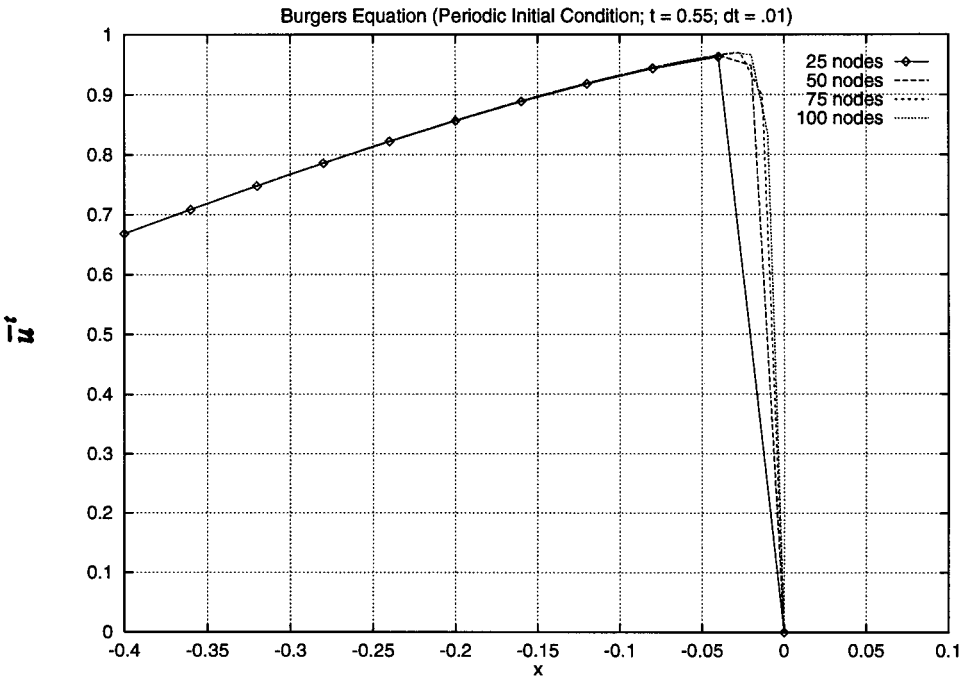

FIG. 14. Solution of the Burgers equation ($\bar{u}^t$ point values) with periodic initial condition ($Re = 100\pi$, $2\tau = 0.01$).

is 151.7491, and the corresponding time $t_{\max}$ is 0.52. The derivative, calculated using the finite difference approach, is 56.3467. With only *two* nodes (and three surfaces) in the narrow region $|x| < 0.02$, and a large time-step of 0.01, the derivative and $t_{\max}$ are in excellent agreement with the exact value, demonstrating the advantage gained by reconstructing the node interior solutions. Also note that a small difference in the NIM result and the exact value is expected, since the exact value is evaluated at a given time, whereas the results of the nodal integral method are averaged over the (last) time interval.

Results shown in Fig. 13, and all other cases solved over the entire domain $x \in [-1, 1]$, showed that symmetry is very well maintained by the MNIM about $x = 0$ for all node sizes and time-steps. For example, $\bar{u}^t$ value at $x = 0$ in Fig. 14 is less than 10^{-29}, and $\bar{u}^t$ value and $\bar{u}^x$ values are symmetric about the $x = 0$ plane. Taking advantage of this property of the MNIM—and the fact

TABLE IV. Maximum derivative and $t_{\max}$ for different node sizes ($Re = 100\pi$).

	$2\tau = \Delta t = 0.01$			$2\tau = \Delta t = 0.005$		
No. of nodes in [0, 1]	$\lvert\frac{\partial u(x=0)}{\partial x}\rvert$			$\lvert\frac{\partial u(x=0)}{\partial x}\rvert$		
	FD approach	Reconstruction	$t_{\max}$	FD approach	Reconstruction	$t_{\max}$
25	24.254	149.0869	0.53	24.2702	149.0698	0.525
50	47.8336	151.5671	0.52	47.9023	151.2248	0.500
75	68.0133	151.8765	0.51	67.9948	151.8643	0.510
100	84.2680	151.9656	0.51	84.2493	151.9513	0.510

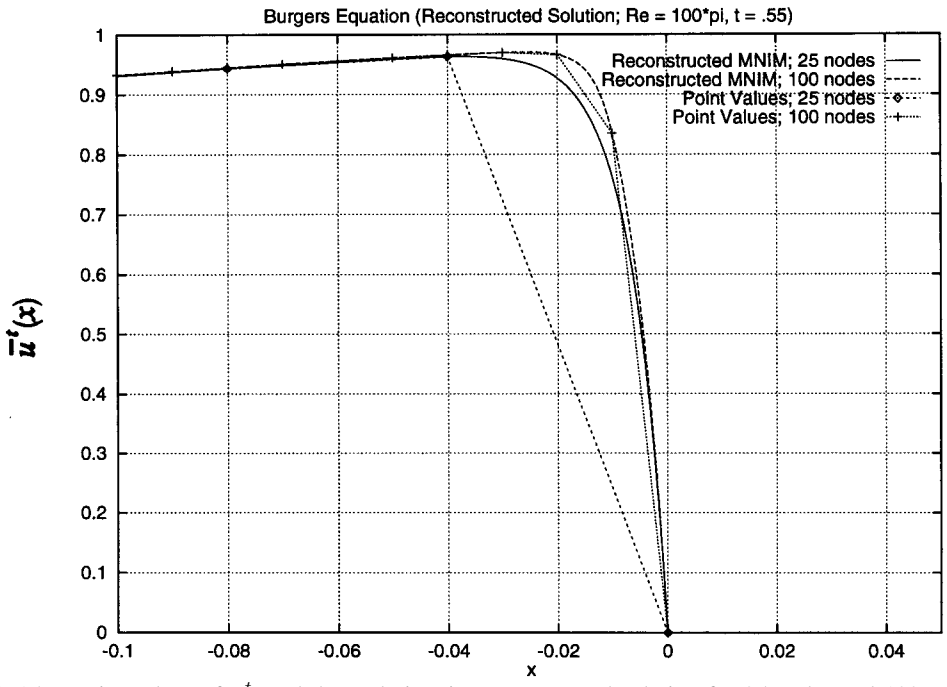

FIG. 15. Point values of $\bar{u}^t$, and the node interior reconstructed solution for 25 nodes and 100 nodes solutions shown in Fig. 14.

that this benchmark problem is sometimes even defined only on [0, 1] [14]—below we solve this problem only on $x \in [-1, 0]$ with $\bar{u}^t(x = 0) = 0$.

To systematically study the effect of number of nodes, we solved the problem with $2\tau = 0.01$, using 25, 50, 75, and 100 nodes (in [0, 1]). Results are shown in Fig. 14, and the maximum of the absolute value of the derivative and $t_{\max}$ are tabulated in Table IV. Clearly, the maximum of the derivative at $x = 0$, even for 100 nodes, if calculated using the finite difference approach is inaccurate, but when calculated by reconstructing the node interior solution in the last node, results of calculation with just 25 nodes and a time-step of 0.01 has less than 2% error. This should be compared with, for example, the Fourier Galerkin approach that yields an error of more than 6% when solved with $\Delta t = 0.003183$ and $N/M = 682/1024$ (2048 grid points over $-1 < x < 1$).

Obviously, the solution in the last node is very different from the straight line that connects the last two $\bar{u}^t$ values for the 25-nodes calculation. The reconstructed solutions [Eq. (31)] for 25 and 100 nodes calculations are plotted in Fig. 15. Though the 25-nodes calculation is not very accurate in predicting the largest velocity and spatial location where it occurs, it accurately follows the 100-node calculation results as x approaches 0, hence, rather accurately predicting the maximum slope.

Next, the effect of time-step size was studied. The results for $\Delta t = 0.005$ are tabulated in Table IV. Contrary to expectations, this finer time-step leads to an increase in the error (by a small amount), suggesting that the error still present is resulting from spatial discretization rather than marching in time. It is also likely that there is error cancellation, since the error introduced by space discretization tends to decrease the derivative, while error introduced due to time-step size tends to increase it (Table IV). Rather than introducing more nodes with uniform node size—which tends to be inefficient as more nodes are introduced even in regions where they are not needed—a simple

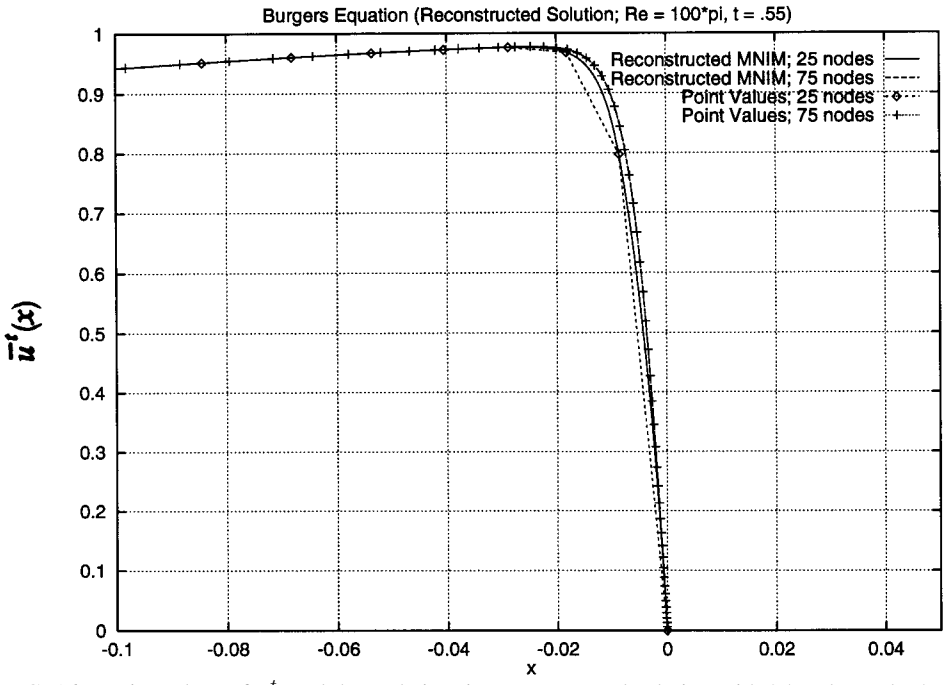

FIG. 16. Point values of $\bar{u}^t$, and the node interior reconstructed solution with 25 nodes and 75 nodes for non-uniform node distribution ($r_x = 0.9$).

scheme was employed to generate non-uniform nodes. Width of nodes decreased geometrically toward the right given by [15]

$$x_{i+1} - x_i = r_x(x_i - x_{i-1}) = r_x\,\Delta x_i, \tag{46}$$

where r_x is the grid growth factor. With a grid growth factor of 0.9, $Re = 100\pi$, and $\Delta t = 0.005$, the problem was solved in the [0, 1] region with 25, 50, and 75 nodes. Results for 25 and 75 nodes calculations are shown in Fig. 16, and the maximum derivative and time reached are tabulated in Table V. While the maximum derivative for uniform node size calculations are less than the exact value, the derivative now (for non-uniform node sizes) is greater than the exact value. For a given number of nodes, there is usually an optimum grid growth factor that yields the best result. The error for this optimum value of r_x is well distributed over the entire domain. Several calculations were carried out with 50 nodes, and $\Delta t = 0.005$, to determine the optimum grid growth factor. Results are tabulated in Table VI. For 50 nodes, with less than 0.01% error, $r_x = 0.96$ appears to be

TABLE V. Maximum derivative and $t_{\max}$ for non-uniform node distribution ($Re = 100\pi$; $2\tau = \Delta t = 0.005$; $r_x = 0.9$).

No. of nodes in [0, 1]	$\lvert\frac{\partial u(x=0)}{\partial x}\rvert$		$t_{\max}$
	FD approach	Reconstruction	
25	93.0678	152.1870	0.510
50	151.6691	152.2684	0.510
75	152.2690	152.2721	0.510

TABLE VI. Maximum derivative and $t_{\max}$ for different grid growth factors, r_x ($Re = 100\pi$; $2\tau = \Delta t = 0.005$; 50 nodes).

Grid growth factor, r_x	$\lvert\frac{\partial u(x=0)}{\partial x}\rvert$		$t_{\max}$
	FD approach	Reconstruction	
0.88	152.2958	152.3912	0.51
0.90	151.6691	152.2684	0.51
0.92	148.8902	152.1619	0.51
0.94	137.9112	152.0840	0.51
0.96	110.6714	152.0199	0.51
0.97	92.7752	151.9790	0.51
1.00	47.9023	151.2248	0.50

the optimum grid growth factor. A final test was carried out to investigate if any of the remaining error resulted from time discretization. This check was especially motivated by the fact that a time-step of 0.005—used in results tabulated in Tables IV–VI—is larger than the time-steps used in all the methods reported in Ref. 16, the smallest used being $0.00015915(\Delta t\pi = 5 \times 10^{-4})$. Results of this last test are tabulated in Table VII. Only minor improvement is noticed in the derivative as Δt is decreased to 0.0001. As stated earlier, a small error in this rather unfair comparison between the exact value at a specific time and the *averaged* value that results from the nodal integral method is expected anyway.

V. DISCUSSION

The modification introduced in the conventional nodal integral method is motivated by the results obtained with the *linear,* steady-state convection–diffusion equation. Introduction of an approximation earlier than usual in the development of the numerical scheme for the nonlinear Burgers equation leads to inherent upwinding similar to that in the linear, steady-state convection–diffusion problem. As is the case in the conventional nodal integral methods, the dependent variable averaged over x for constant time, and the dependent variable averaged over time for constant x are determined. Along with averaged quantities on nodes surfaces, reconstruction of node interior distributions results automatically. For Burgers equation, time-averaged (over 2τ) space-dependent velocity, and space-averaged time-dependent velocity $[\bar{u}^t(x)$ and $\bar{u}^x(t)]$ in the interior of each node are reconstructed.

Application of the MNIM to the steady-state Burgers equation confirmed that the method is $O(a^2)$. Solution of the modified propagating shock wave problem for a large number of spatial

TABLE VII. Maximum derivative and $t_{\max}$ for different time-step, 2τ ($Re = 100\pi$; 50 nodes; $r_x = 0.96$).

Time step (2τ)	$\lvert\frac{\partial u(x=0)}{\partial x}\rvert$		$t_{\max}$
	FD approach	Reconstruction	
0.005	110.6714	152.0199	0.510
0.003	110.6655	152.0162	0.510
0.001	110.6603	152.0138	0.510
0.0001	110.6595	152.0134	0.5097

nodes and one time-step showed that the method is $O(\tau^2)$. The inherent upwinding and the node interior reconstruction capability of MNIM are further demonstrated by solving the periodic initial condition problem for a rather large Reynolds number. The modified NIM with only 50 nodes yields a rather accurate value for a very sensitive measure of accuracy for this problem. Like all other schemes [16], MNIM also can be improved by non-uniform grid distribution to roughly the same accuracy as some of the best schemes employed to solve this problem; ABCN (collocation, Chebyshev), ABCN spectral. MNIM performs better than many other schemes such as Fourier Galerkin, Fourier pseudo-spectral and finite difference [16]. Furthermore, the conventional and modified NIMs do not introduce any *ad hoc* dissipativity term as used in some other schemes [16]. Numerical optimization was introduced only to determine the optimal grid growth factor. Further improvement in results can be achieved by optimizing the coordinate transformation scheme.

Reconstruction of the node interior solution was demonstrated by solving the above problem on a very coarse grid and then reconstructing the solution. The reconstructed solution—in the node with the largest change in u—demonstrates the significant advantage NIMs have over finite difference scheme.

This work was supported by NASA under grant number NAGW/3021.

VI. SUMMARY

A modified nodal integral method is proposed and developed for Burgers equation. By introducing an approximation early in the development, the resulting modified nodal integral method has inherent upwinding, is second order in both space and time, and shows excellent accuracy for two rather difficult problems. Without any artificial viscosity added, the new method is capable of very efficiently suppressing spurious oscillations that plague other schemes.

APPENDIX A: APPLICATION OF THE CONVENTIONAL NODAL INTEGRAL METHOD (NIM) TO THE BURGERS EQUATION [4]

Equations (2) and (6–8) in the main text of this article do not change for the conventional NIM. Equation (3) of the main text is written differently in the conventional method—absorbing the nonlinear term in the pseudo-source term $\bar{S}_2^t(x)$:

$$\frac{1}{Re}\frac{d^2\bar{u}^t(x)}{dx^2} = \bar{S}_2^t(x) \equiv \frac{1}{(2\tau)}\int_{-\tau}^{+\tau}\left[\frac{\partial u(x,t)}{\partial t} + u(x,t)\frac{\partial u(x,t)}{\partial x}\right] dt. \tag{A.1}$$

After expanding and truncating the pseudo-source term $\bar{S}_2^t(x)$, Eq. (A.1) is solved:

$$\begin{aligned}\bar{u}_{i,j}^t(x) \;=\; & \bar{u}_{i,j}^t(-a_{i,j}) + \left[\frac{d\bar{u}_{i,j}^t(-a_{i,j})}{dx} + Rea_{i,j}\bar{S}_{2,(i,j)}^{tx}\right](x + a_{i,j}) \\ & + \left(\frac{Re\bar{S}_{2,(i,j)}^{tx}}{2}\right)(x^2 - a_{i,j}^2).\end{aligned} \tag{A.2}$$

Omitting the details associated with equating the spatial derivative of the velocity on the two sides of an interface between node i and $(i+1)$—corresponding to Eqs. (11)–(13) in the main text—we

arrive at the three-point scheme in terms of the pseudo-sources in node i and $(i+1)$:

$$\left(\frac{1}{a_{i,j}}\right)\bar{u}^t_{i-1,j} - \left(\frac{1}{a_{i,j}} - \frac{1}{a_{i+1,j}}\right)\bar{u}^t_{i,j} + \left(\frac{1}{a_{i+1,j}}\right)\bar{u}^t_{i+1,j}$$

$$= \; 2\, Re[a_{i,j}\bar{S}^{tx}_{2,(i,j)} + a_{i+1,j}\bar{S}^{tx}_{2,(i+1,j)}]. \tag{A.3}$$

Equation (A.3) corresponds to Eq. (14) in the main text. The ''conservation of sources'' equation for the conventional NIM, obtained by integrating the Burgers equation over the node, is

$$\bar{S}^{xt}_1 - \bar{S}^{tx}_2 + \frac{1}{2}\frac{\overline{\partial u^2}^{tx}}{\partial x} = 0. \tag{A.4}$$

The last term in Eq. (A.4) is approximated by $\frac{1}{2}\frac{\overline{\partial(\bar{u}^t)^2}^x}{\partial x}$, which leads to a second order error. The last constraint equation is obtained by setting

$$\bar{u}^{tx}_{i,j} = \bar{u}^{xt}_{i,j}, \tag{A.5}$$

where $\bar{u}^{xt}_{i,j}$ is given by Eq. (17), as

$$\bar{u}^{xt}_{i,j} = \bar{u}^x_{i,j-1} + \tau\bar{S}^{xt}_{1,(i,j)}, \tag{A.6}$$

and $\bar{u}^{tx}_{i,j}$ is obtained by integrating Eq. (A.2), which yields

$$\bar{u}^{tx}_{i,j} = \left(\frac{\bar{u}^t_{i,j} + \bar{u}^t_{i-1,j}}{2}\right) - Re\left(\frac{a^2_{i,j}}{3}\right)\bar{S}^{tx}_{2,(i,j)}. \tag{A.7}$$

Solving Eqs. (8), (A.3), (A.4), and (A.5), and eliminating $\bar{S}^{xt}_{1,(i,j)}$ and $\bar{S}^{tx}_{2,(i,j)}$, the final set of two equations [4] for the two unknowns per node is (for all equal size nodes):

$$\left(\frac{\bar{u}^x_{i,j} - \bar{u}^x_{i,j-1}}{2\tau}\right) + \frac{1}{4a}(\bar{u}^{t^2}_{i,j} - \bar{u}^{t^2}_{i-1,j}) - \frac{3}{2a^2 Re}\{\bar{u}^t_{i,j} + \bar{u}^t_{i-1,j} - \bar{u}^x_{i,j} - \bar{u}^x_{i,j-1}\} = 0 \tag{A.8}$$

and

$$\bar{u}^t_{i-1,j} + 4\bar{u}^t_{i,j} + \bar{u}^t_{i+1,j} - \frac{3}{2}\{\bar{u}^x_{i,j} + \bar{u}^x_{i+1,j} + \bar{u}^x_{i,j-1} + \bar{u}^x_{i+1,j-1}\} = 0. \tag{A.9}$$

Equation (A.8) corresponds to Eq. (20), and Eq. (A.9) corresponds to Eq. (21) of the modified NIM approach.

APPENDIX B: SMALL CELL REYNOLDS NUMBER LIMIT

In this appendix we show that the modified nodal integral method is actually a generalization of the conventional NIM, and it actually reduces to the latter in the limit of small cell Reynolds number. It is shown for uniform grid spacing, $a_{i,j} = a$. The goal is, hence, to show that for small cell Reynolds number $(2a\ u\ Re)$, Eqs. (20) and (21) actually reduce to Eq. (A.8) and Eq. (A.9). This is an exercise in repeated application of l'Hospital rule.

Note that the Taylor expansion for small y for $f_1(y) = \frac{y}{1-e^{-by}}$, is

$$f_1(y) = \frac{1}{b} + \frac{1}{2}y + \frac{b}{12}y^2 + \cdots. \tag{B.1}$$

and

$$f_2(y) = \frac{y}{e^{by} - 1} = \frac{1}{b} - \frac{1}{2}y + \frac{b}{12}y^2 + \cdots, \tag{B.2}$$

where, for our purpose, $b = 1$ and $y = 2a\ u^0_{i,j}\ Re$. Assuming $(2a\ u^0_{i,j}\ Re)$ to be small (recall that $u^0_{i,j}$ was assumed to be the constant velocity over the node (i, j), equal to the average $((\bar{u}^t_{i,j} + \bar{u}^t_{i-1,j})/2)$) and applying Eqs. (B.1) and (B.2) to $A_{i,j}, B_{i,j}, \ldots, I_{i,j}$, we get

$$Reu^0_{i,j} H_{i,j} = \frac{1}{2a} - \frac{1}{2}Reu^0_{i,j} + \frac{a}{6}\,(Reu^0_{i,j})^2 + \cdots$$

$$Reu^0_{i,j} I_{i,j} = \frac{1}{2a} + \frac{1}{2}Reu^0_{i,j} + \frac{a}{6}\,(Reu^0_{i,j})^2 + \cdots$$

$$G_{i,j} = a + \frac{a^2}{3}Reu^0_{i,j} + \cdots$$

$$A_{i,j} = \frac{1}{2} - \frac{a}{6}\,(Reu^0_{i,j}) + \cdots$$

$$B_{i,j} = \frac{1}{2} + \frac{a}{6}\,(Reu^0_{i,j}) + \cdots$$

$$\frac{C_{i,j}}{Re} = -\frac{a^2}{3} + \cdots$$

$$D_{i,j} = -\left(\frac{1}{a} + \frac{Reu^0_{i,j}}{2}\right) + \cdots$$

$$E_{i,j} = -\frac{4}{a} + \frac{Re}{2}(u^0_{i+1,j} - u^0_{i,j})$$

$$F_{i,j} = \frac{Reu^0_{i,j}}{2} - \frac{1}{a}.$$

Substituting $A_{i,j}, B_{i,j}, \ldots, I_{i,j}$ in Eqs. (20) and (21), realizing that $u^0_{i,j} = (\bar{u}^t_{i,j} + \bar{u}^t_{i-1,j})/2$, and simplifying results in Eqs. (A.8) and (A.9).

APPENDIX C: TIME-AVERAGED AND SPACE-AVERAGED EXACT SOLUTION OF THE MODIFIED PROPAGATING WAVE PROBLEM

The exact solution for the modified propagating wave problem (Section IVB) is given by Eq. (43). The space-averaged solution (over a node) is:

$$\begin{aligned}\bar{u}^x(t) &\equiv \frac{1}{2a_{i,j}}\int_{x_\ell}^{x_r} u(x,t)\,dx \\ &= 0.5 - \frac{1}{(a_{i,j}Re)}\left\{\ln\left[\cosh\left(\frac{Re}{4}\left(x_r - \frac{t}{2}\right)\right)\right]\right. \\ &\quad \left. - \ln\left[\cosh\left(\frac{Re}{4}\left(x_l - \frac{t}{2}\right)\right)\right]\right\}, \end{aligned} \tag{C.1}$$

where x_ℓ and x_r are the left and right boundaries of the node. The time-averaged solution (over a time-step 2τ; from $(t_f - 2\tau)$ to t_f) is

$$\begin{aligned}\bar{u}^t(x) &\equiv \frac{1}{(2\tau)}\int_{t_f-2\tau}^{t_f} u(x,t)\,dt \\ &= 0.5 + \frac{2}{(Re\tau)}\left\{\ln\left[\cosh\left(\frac{Re}{4}\left(x - \frac{t_f}{2}\right)\right)\right]\right. \\ &\quad \left. - \ln\left[\cosh\left(\frac{Re}{4}\left(x - \frac{(t_f - 2\tau)}{2}\right)\right)\right]\right\}. \end{aligned} \tag{C.2}$$

References

1. E. P. E. Michael, J. J. Dorning, E. M. Gelbard, and Rizwan-uddin, ''A nodal integral method for the convection–diffusion heat equation,'' *Trans. Am. Nucl. Soc.* **69,** 239–241 (1993).
2. E. P. E. Michael, J. J. Dorning, and Rizwan-uddin, ''A third order nodal integral method for the convection–diffusion equation,'' *Trans. Am. Nucl. Soc.* **71,** 195–197 (1994).
3. C. A. J. Fletcher, ''Burgers' equation: a model for all reasons,'' in *Numerical Solutions of Partial Differential Equations,* John Noye, Ed., North–Holland, Amsterdam, 1981, pp. 355–475.
4. W. J. Decker, ''A block iterative nodal-integral method for fluid dynamics problems,'' M. S. Thesis, University of Virginia, 1995.
5. T. J. Burns and J. J. Dorning, ''A new computational method for the solution of multidimensional neutron diffusion problems,'' in *Proc. of the Joint NEACRP/CSNI Specialists' Meeting on New Developments in Three-Dimensional Neutron Kinetics and Review of Kinetics Benchmark Calculations,* Garching, Munich, Germany, 1975, pp. 109–130. Laboratorium fur Reaktorregelung and Anlagensicherung.
6. William C. Horak, ''Local Green's functions techniques for the solution of heat conduction and incompressible fluid flow problems,'' Ph. D. thesis, University of Illinois, 1980.
7. W. C. Horak and J. J. Dorning, ''A nodal coarse-mesh method for the efficient numerical solution of laminar flow problems,'' *J. Comp. Physics* **59,** 405–440 (1985).
8. R. D. Lawrence and J. J. Dorning, ''A nodal green's function method for multidimensional neutron diffusion calculations,'' *Nuclear Sci. Eng.* **76,** 218–231 (1980).
9. Y. Y. Azmy, ''A nodal integral method for the numerical solution of incompressible fluid flow problems,'' Master's Thesis, University of Illinois, 1982.
10. Y. Y. Azmy and J. J. Dorning, ''A nodal integral approach to the numerical solution of partial differential equations,'' in *Advances in Reactor Computations,* Vol. II, American Nuclear Society, LaGrange Park, IL, 1983, pp. 893–909.
11. Gary Wilson, ''Time-dependent nodal integral method,'' Ph. D. thesis, University of Virginia, 1987.

12. G. L. Wilson, R. A. Rydin, and Y. Y. Azmy, ''Time-dependent nodal integral method for the investigation of bifurcation and nonlinear phenomena in fluid flow and natural convection,'' *Nucl. Sci. Eng.* **100,** 414–425 (1988).

13. C. A. J. Fletcher, ''A comparison of finite element and finite difference solutions of the one- and two-dimensional Burgers' equations,'' *J. Comp. Physics* **51,** 159–188 (1983).

14. P. L. Sachdev, *Nonlinear Diffusive Waves,* Cambridge University Press, New York, 1987.

15. C. A. J. Fletcher, *Computational Techniques for Fluid Dynamics I,* Springer, New York, 1988.

16. C. Basdevant, M. Deville, P. Haldenwang, J. M. Lacroix, J. Ouazzani, R. Peyret, P. Orlandi, and A. T. Patera, ''Spectral and finite difference solutions of the Burgers' equation,'' *Computers & Fluids* **14,** 23–41 (1986).

17. D. G. Cacuci and O. A. Karakashian, ''Benchmarking the propagator method for nonlinear systems: a Burgers–Korteweg–deVries equation,'' *J. Comp. Physics* **89,** 63–79 (1990).